3-10-1999

Surficial slip distribution on the central Emerson fault during the June 28, 1992, Landers earthquake, California

Sally F. McGill

Charles M. Rubin

JOURNAL OF GEOPHYSICAL RESEARCH, VOL. 104, NO. B3, PAGES 4811-4833, MARCH 10, 1999

Surficial slip distribution on the central Emerson fault during the June 28, 1992, Landers earthquake, California

Sally F. McGill

Department of Geological Sciences, California State University, San Bernardino

Charles M. Rubin

Department of Geology, Central Washington University, Ellensburg

Abstract. We present the results of our mapping of a 5.6-km length of the central Emerson fault that ruptured during the 1992 Landers earthquake in the southwestern Mojave Desert, California. The right-lateral slip along this portion of the rupture varied from about 150 to 530 cm along the main rupture zone. In some locations a total of up to 110 cm of additional right-lateral slip occurred on secondary faults up to 1.7 km away from the main rupture zone. Other secondary faults carried up to several tens of centimeters of left-lateral or thrust displacement. The maximum net vertical displacement was 175 cm, east-side-up. The sense of vertical slip across the main fault zone varied along strike, but in most cases it was consistent with the sense of vertical slip in previous earthquakes, as indicated by the locations of areas of older, uplifted, and abandoned alluvial fan surfaces. Although variations in surficial slip have been reported along previous strike-slip ruptures, our closely spaced slip measurements allow a much more detailed study of slip variability than was possible previously. We document variations in slip as large as 1 m or more over distances ranging from 1-2 km to a few tens of meters, suggesting that strains of the order of 10^{-1} may have occurred locally within the surficial sediments. The long-wavelength (kilometer-scale) variations in surficial slip may be influenced by fault geometry and perhaps by the thickness of unconsolidated sediments. The slip variations over shorter length scales (tens of meters) may be caused by variations in the proportion of the total shear that occurs on visible, brittle fractures versus that which occurs as distributed shear, warping or rotation. The variability of slip along the ruptures associated with the Landers earthquake calls for caution in interpreting geomorphic offsets along prehistoric fault ruptures.

1. Introduction

The M_w 7.3 Landers earthquake of June 28, 1992, was produced by a northward propagating pulse of right-lateral slip on five major faults that totaled about 85 km in length [*Sieh et al.*, 1993]. To document the slip and variability of slip along the rupture, we mapped a 5.6-km length of the surficial ruptures along the Emerson fault, southeastward from the location of the maximum horizontal displacement at Galway Lake Road (Figure 1). Horizontal and vertical slip across the faults was measured wherever linear features of cultural or natural origin crossed the fault zone, with a typical spacing of a few tens of meters. We document a high degree of variability in the lateral slip over several distance scales.

Previous investigations of other large, historical, strike-slip ruptures had reported slip variability over distances of hundreds of meters to kilometers [*Ambraseys and Tchalenko*, 1969; *Ambraseys and Zatopek*, 1969; *Bucknam et al.*, 1978; *Nowroozi and Mohajer-Ashjai*, 1980/1981; *Sharp*, 1982; *Sharp et al.*, 1982; *Thatcher and Lisowski*, 1987; *Toksoz et al.*, 1977], but slip measurements < 50 m apart on historical strike-slip ruptures had never been reported. Interpretations of slip measurements along prehistoric ruptures have been hindered by the sparse distribution of displacement measurements along historical ruptures [*McGill and Sieh*, 1991]. The densely spaced displacement measurements reported here will facilitate studies of prehistoric ruptures by providing an example of the small-scale variations in slip that may occur along earthquake ruptures.

Paper number 98JB01556.
0148-0227/99/98JB-01556$09.00

2. Methodology

We spent 3 weeks in the field, mapping surficial fault ruptures onto 1:6000 scale air photos and measuring displacements across the fault (Plate 1). We chose to focus on fractures with ≥ 10 cm of displacement, and we mapped every such fracture that we found. We also mapped many fractures with smaller displacements, particularly if they had larger displacements elsewhere along their length.

We made 60 slip measurements across the main fault zone (Table 1) and nearly 200 measurements across secondary fault

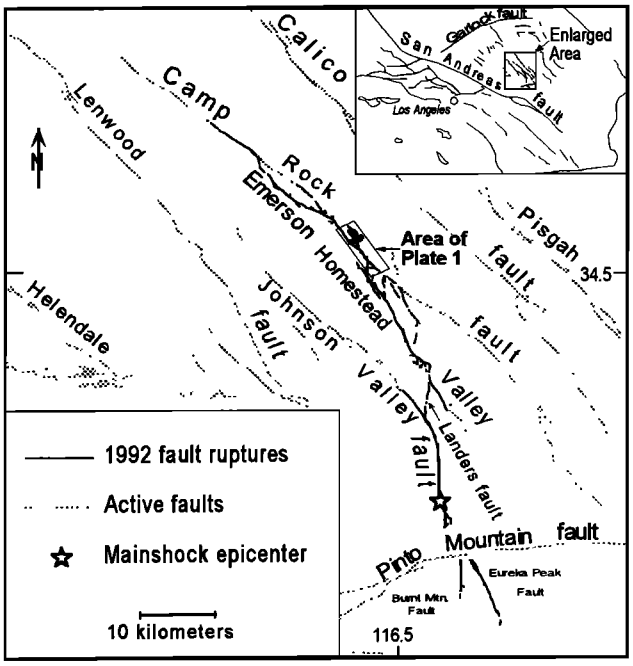

Figure 1. Location map showing the Landers earthquake rupture [after *Sieh et al.*,1993] and active faults in the southwestern Mojave Desert, California.

traces up to 1.7 km from the main trace (Table 2). We supplemented these with 24 measurements made by other scientists (see acknowledgments). Lateral displacements were measured from offsets in linear reference features such as off-road vehicle tracks, ephemeral stream channels, gullies, ridges, and a few dirt roads (Figure 2). The secondary faults away from the main fault zone were usually very simple; geomorphic or cultural features were usually cleanly offset across a single fracture, and displacements could usually be measured to within a few centimeters. The main fault zone typically consisted of one or two main fault traces or shear zones and a several-meter-wide zone of fractures with smaller displacements between and on either side of the main trace(s). The wider zone of displacement along the main fault led to greater uncertainties in the displacements across the main fault. The slip measurements across the main fault zone include slip across all visible fractures within a zone several tens of meters wide, centered on the main fault trace(s). In a few cases, slip was measured on linear features that did not span the entire width of the main fault zone, but these are reported as minima.

Offsets were measured with a steel tape. The uncertainty in the measurement usually stemmed from having to project the offset feature through the several-meter-wide fault zone, where the feature had been disrupted. The offset features did not always have the same trend on either side of the fault zone, and different assumptions about the trend of the offset feature through the fault zone led to different slip estimates.

A significant amount of lateral displacement may have occurred as warping in addition to brittle slip on visible fractures. For example, a power line crosses the northern Emerson fault, north of the area that we mapped. The lateral slip on visible cracks at this site was 250 cm, whereas offset of the aligned power line towers (including lateral warping away from the fault) was 345 cm [*Yeats et al.*, 1997; see also *Lazarte et al.*, 1994]. Because the offset features we used were not perfectly linear prior to the earthquake, it was not possible to include lateral warping away from the main fault trace(s) in our measurements, except for our surveyed measurement of the offset of Galway Lake Road (discussed in section 3.1). Our measurements thus are lower bounds on the total deformation but are useful for comparison to offsets along prehistoric ruptures, where warping is equally difficult to detect or measure.

3. General Observations About the Ruptures

The right-lateral slip along the main fault zone varied from 150 ± 30 cm to 531± 62 cm, and the net vertical slip varied from 175 ± 15 cm, east-side-up, to 50 cm, west-side-up (Figure 3). The variability in slip is discussed in more detail in section 5.

3.1. Maximum Lateral Offset at Galway Lake Road

One of the largest lateral offsets on the main fault zone was located where the dirt road diverging from Bessemer Mine Road toward Galway Lake crosses the fault (sites 3-6, Plate 1; see photo 2 of *Hart et al.* [1993]). On the day after the earthquake, K. Sieh, K. Hudnut, and C. Rubin used a steel tape to measure right-lateral offsets ranging from 570 to 677 cm on several linear features associated with this road.

In order to rigorously document this very large offset, we used a Wild TC1010 total station to survey points along the road edges, berms, and major fault traces (Figure 4). To measure the right-lateral offset of each reference feature, we first rotated and translated the surveyed coordinates so that the y axis is parallel to and centered within the fault zone. Using a linear regression routine, we projected the road edges and berms on each side of the fault separately to the center of the fault zone. The difference between the y intercepts of the regression lines for the same feature on opposite sides of the fault is the lateral offset. The surveyed offset measurements (409 to 531 cm) are somewhat smaller than those measured with a steel tape the day after the earthquake (Table 3). U.S. Geological Survey scientists also surveyed the Galway Lake Road after the earthquake. They estimate an average of 520 cm for the right-lateral offset of this road (D. Ponti, written communication, 1993) (see Table 3). The fact that neither the road nor the fault is perfectly straight introduces errors into the projection, which can lead to rather large errors in the slip measurements. This may account for the discrepancies between offsets measured by different investigators at this site.

3.2. Vertical Slip

Although vertical slip was east-side-up along most of the fault length that we studied, west-side-up displacement was observed in a few places. With few exceptions (e.g., at about 3.5 km) the sense of vertical displacement along the fault in 1992 was consistent with the sense of vertical slip in prior earthquakes, as indicated by the locations of uplifted, older alluvial fans, and Plio-Pleistocene sediments (Plate 1 and Figure 3d).

3.3. Nature of the Fault Scarps

Free faces were present along most of the portion of 1992 fault rupture that had significant vertical slip. Where the rupture offset indurated sediments, the free face was particu-

Table 1. Offsets Along the Main Fault Rupture

Site			Right-Lateral Slip		Vertical	
Plate 1	Field Notes	Distance,[a] km	Main Zone, cm	Other Fractures,[b] cm	Slip,[c] cm	Description
1	SM83	-0.29	310 ± 45	63 ± 21	46 ± 10 ESU	center of sandy channel.
2	SM82	-0.10	380 ± 45	48 ± 8	40 ± 14 ESU	motorcycle track
3a	SM251	-0.010	409 ± 175[d]	48 ± 8	24 ± 25 ESU	North edge of North berm, Galway Lake Road
3	SM250	-0.007	471 ± 125[d]	48 ± 8	44 ± 67 ESU	South edge of North berm, Galway Lake Road
4	SM249	0.0	531 ± 62[d]	48 ± 8	22 ± 14 WSU	North edge of central berm, Galway Lake Road
5	SM248	0.003	466 ± 35[d]	48 ± 8	12 ± 14 WSU	South edge of central berm, Galway Lake Road
6	SM247	0.007	414 ± 47[d]	48 ± 8	14 ± 15 ESU	South edge of Galway Lake Road
7	CR17	0.33	500 ± 50	110 ± 51	25 WSU	tire track
8	CR4	0.67	530	76 ± 33	0	tire track
9	SM73b	0.76	380 ± 71	64 ± 8	ESU	old tire track
10	SM74	0.81	355 ± 115	64 ± 4	ESU	three parallel ruts
11	SM75	0.86	230 $\pm^{66}_{49}$	63 ± 8	55±20 ESU	gully
12	CR5	0.88	500	72 ± 14	> 90 ESU	gully
13	SM76	0.93	400 $\pm^{50}_{150}$	72 ± 14	135±20 ESU	incised part of sandy channel
14	SM77	0.96	375 ± 55	8 ± 19	120 ESU	NW edge of channel
15	SM78	0.99	355 ± 55	8 ± 19	130 ± 10 ESU	Center of incised sandy channel
16	SM79	1.05	415 ± 30	26 ± 10	130 ± 10 ESU	SE edge of incised sandy channel
17	SM80	1.07	380 ± 25	26 ± 10	170 ± 11 ESU	gully
18	SM81/CR6	1.10	410 $\pm^{60}_{20}$	34 ± 11	175±11 ESU	single, wide tire rut
19	CR7	1.44	335 ± 50	19 ± 8	150 ESU	ridge crest
20	CR8	1.61	220	23 ± 22	20 WSU	
21	CR10	1.99	≥ 170	54 ± 37	20 ESU	channel
22	SM31	2.14	225 ± 21	69 ± 15	54 ± 3 ESU	NW edge of small channel
23	SM4	2.17	245 $\pm^{15}_{25}$	60 ± 17	85 ± 5 ESU	NW edge of sandy channel
24	SM32	2.18	150 ± 30	60 ± 17	68 ± 2 ESU	NW edge of sandy channel
25	SM33/CR11	2.26	390 ± 23	63 ± 12	80 ± 10 ESU	NW edge of sandy channel
26	SM34	2.38	225 ± 25	74 ± 10	25 ± 5 ESU	NW edge of sandy channel
27	SM90	2.40	230 $\pm^{102}_{46}$	101 ± 18	70 ± 15 ESU	channel warped, not broken
28	CR12	2.65		0	110 ESU	scarp; warped, not broken
29	SM35	2.73	≥ 205±30	0	30 ± 5 ESU	SE edge of sandy channel
30	CR13	2.76	≥ 250	0	40 ESU	grass line adjacent to NW channel edge
31	SM36	2.79	330 ± 100	0	ESU	NW and SE edge of sandy channel
32	SM38	2.95	220 ± 100	0	35 ESU	sandy channel warped
33	CR15	3.00	340	22 ± 22		SE edge of small, sandy channel
34	SM39	3.058	240	45 ± 25	40 ESU	sandy channel warped
35	SM40	3.07	375 ± 35	45 ± 25	70 ESU	sandy channel warped
36	SM41	3.11	220 $\pm^{50}_{75}$ [d]	28 ± 18	85 ± 5 ESU	channel offset on four discrete fractures
37	SM42	3.12	375 ± 60[d]	10 ± 5	100 ESU	sandy channel offset
38	SM43&44 (net)	3.26	411 ± 25	17 ± 2	69 ± 8 ESU	cycle track
39	SM45&46 (net)	3.33	296 ± 14	9± 9	65 ± 15 ESU	cycle track
40	SM47	3.5	≥ 112	8± 1	30 WSU	NW edge of channel; does not cross entire main trace
41	CR16	3.61	433 ± 25	1 ± 1	30 WSU	dirt road with ruts
42	SM98	3.63	389 ±30	4± 1	< 20	single tire track
43	SM99	3.67	417 ± 40	13 ± 3	8 ± 11 WSU	50-70-cm-wide track
44	SM100	3.73	345 ± 18	6 ± 6	0	30-40-cm-wide tire track
45	SM102	3.80	436 ± 28	0	0 ± 11	40-cm-wide rut
46	CR18	4.04	≥ 230	0	45 ESU	NW side of motorcycle track
47	SM103	4.10	408 ± 28	14 ± 1	23 ± 10 ESU	single tire track
48	SM104/CR19	4.13	355 ± 60	16± 2	30 ESU	40-cm-wide track
49	SM105	4.29	345 ± 35	25 ± 1	20 ± 12 ESU	40-cm-wide track
50	CR20	4.33	≥ 190	48± 6	202 ± 13 ESU[e]	pebble lag tire track
51	SM106	4.43	195 ± 58	20 ± 2	5 ESU	70-cm-wide track
52	CR21	4.60	320	49 ± 10		track
53	CR34	4.62	211	32 ± 4	15 WSU	channel
54	CR35	4.64	276	14 ± 2	50 WSU	center line of narrow, cobble-rich channel
55	CR24	4.69	≥ 110	14 ± 2		NW edge of channel wall
56	CR36	4.76	260 ± 18	0	22 ESU	sandy channel
57	CR25	4.90	≥ 191	136 ± 47[f]	133 ESU?	dirt road
58	CR26	5.02	152	215 ± 36[f]	78 ESU	cycle track
59	CR37	5.08	229 ± 21	109 ± 10[f]	100 ± 5 ESU	cycle track
60	CR27	5.32	≥ 110 ±30	98 ± 10[f]		channel

[a] Distances measured southeastward along fault from Galway Lake Road.

[b] A line perpendicular to the main fault trace was drawn through each slip measurement on the main fault trace. Where these lines crossed secondary fault traces, slip values were interpolated from the nearest two measurements on the secondary fault trace, and the component of slip parallel to the main fault was computed. These values were then summed to obtain the number reported.

[c] ESU, east side up; WSU west side up.

[d] Surveyed measurement. All other measurements were by steel tape.

[e] The net vertical slip is 132 cm ESU because 70 ± 4 cm WSU slip occurred on secondary fractures.

[f] Includes slip on the Homestead Valley fault [*Zachariasen and Sieh*, 1995].

Table 2. Offsets on Secondary Fractures

Site		Right Lateral	Vertical	
Plate 1	Field Notes	Slip, cm	Slip,[a] cm	Description
100	sm-223	18 ± 8		channel
101	sm-222a	6 ± 3	2 ± 2	narrow tire track
102	sm-222b	15 ± 5	-10 ± 5	
103	sm-233	15 ± 5	0 ± 2	channel edge
104	sm-221	15 ± 5	-15 ± 3	wide tire track
104b	sm-221b	≤ 5	4 ± 2	
105	sm-220	15 ± 5	-19 ± 1	tire track
105b	sm-220b	8 ± 5	11 ± 1	same tire track as 105
106	sm-232	7 ± 5	0 ± 2	channel
107	sm-219	17 ± 5	-6 ± 1	narrow tire track
108	sm-218	15 ± 5	0 ± 3	narrow tire track
109	sm-244a	30 ± 10	-15 ± 3	tire tracks
110	sm-243	60 ± 10	0	tire track
111	sm-207	12 ± 5	-3 ± 2	channel
112	sm-231	13 ± 3	0 ± 3	two narrow tire tracks
113	sm-217a	14 ± 4	-2 ± 2	narrow tire track
114	sm-217b	6 ± 4	0 ± 3	narrow tire track
115	sm-206	20 ± 20	-10 ± 5 T[b]	tire track
116	sm-242	20 ± 5	0	tire track
117	sm-230	10 ± 5	0 ± 2	channel
118	sm-205	2 ± 1	0	small pull-aparts
119	sm-203	2	0	small pull-apart
120	sm-204	0 ± 5	-10 ± 5 T	tire track
121	sm-229	13 ± 3	0 ± 2	channel
122	sm-202	1	0	small pull-apart
123	sm-241	10 ± 5	5 ± 3	tire track
124	sm-228	30 ± 15	0 ± 2	wide tire track and channel
125	sm-240	30 ± 10		tire track
126	dy-2	33 ± 10	- 2 ± 1	
127e	sm-239e	30 ± 5	0	berm
127c	sm-239c	30 ± 15	-5 ± 5	berm
127b	sm-239b	-5 ± 3	0	berm
127d	sm-239d	5 ± 3	0	berm
127a	sm-239a	44 ± 5	-15 ± 10	berm
127f	sm-239f	5 ± 3	0	berm
128	sm-226	5 ± 3	0 ± 2	two tire tracks
129	sm-225	1 ± 1	1± 1	several tire tracks
130	dy-1	41 ± 3	-2 ± 2	roots
131a	sm-238a	45 ± 10	-13 ± 3	
131b	sm-238b	5 ± 2	0	
132	dy-3	13		small pull-apart
133	sm-237	75 ± 35	0 ± 5	channel
134	jl-9		-7 ± 5 T	
138	sm-201	-20 ± 3	0 ± 3	channel
139	sm-214	-15 ± 5	-5 ± 3	tire track
140	sm-215	-7 ± 2	3 ± 1	narrow tire track
141	sm-211	-15 ± 5	0 ± 2	channel
142	sm-212	-4 ± 2	0 ± 3	two channels and small pull-apart
143	sm-213	-5 ± 3	0 ± 3	three tire tracks
144	jl-8	10 ± 5	-11 ± 2	
145	sm-210e	-15 ± 3	-3 ± 3	tire track
146	sm-210w	-10 ± 3	-4 ± 2	tire track
147	sm-235	2 ± 2	2.5 ± 1	tire track
148	sm-209	-15 ± 5	-8 ± 3	tire track
149	jl-6	4 ± 1	-1 ± 0.5	
150	sm-236	65 ± 5	0 ± 5	berm at north edge of road
151	jl-11	-135 ± 10	7 ± 3	
152	jl-7	15 ± 5	-10 ± 1	
153	sm-48	75 ± 10	-15 ± 5	berm at south edge of road
154	sm-208	-27 ± 5	-5 ± 3	tire track
155	jl-13		2 ± 1	
156	sm-84	-38 ± 5	-13 ± 2	tire track
157	sm-200	10 ± 5	-3 ± 1	channel
158	sm-49	75 ± 10	-10 ± 5	channel
159	jl-5	55 ± 10	-18 ± 2	
160	jl-4	3 ± 1	0	
161	jl-3	-30 ± 10	0	
162	sm-50	47 ± 5	0 ± 2	small pull-aparts
163	jl-2	1 ± 0.5	0	
164	sm-51	4 ± 1		small pull-apart
165	jl-1	-7 ± 2	0	
166	jl-14	22 ± 2	1 ± 0.5	
167	sm-52	8 ± 3	0	small pull-aparts
168	sm-123	8 ± 8	0 ± 10	
169	sm-128	-50 ± 5	-10 ± 3	wide track
170	sm-53	2 ± 1		small pull-aparts
171	cr-33	10.5		center berm of road
172	sm-54	10 ± 5	0 ± 2	channel
173	sm-148	0 ± 10	-5 T	tire track
174	sm-150	9 ± 1	-5 ± 1	narrow tire track
175	sm-122	0 ± 5	0 ± 3	
176	cr-17			
177	sm-130	10 ± 10	0 ± 3	tire track
178	sm-129	-40 ± 10	-5 ± 5	tire track
178b	sm-96	25 ± 5	-10 ± 5	tire track
179	sm-55	10 ± 1		small pull-apart
180	sm-151	0 ± 5	-15 ± 2	channel
181	sm-149		≤ 15	
182	sm-121	32 ± 5	-20 ± 5	tire track
183	sm-85	25 ± 5	-5 ± 1	tire track
184	sm-124	33 ± 5	-15 ± 3	channel
185	sm-56		-25 T	
186	sm-152	0 ± 5	-4 ± 1	channel
187	sm-58	0 ± 5	-5 ± 1T	
188	sm-59	0 ± 10	-25 ± 5	channel
189	sm-120	65 ± 10	-20 ± 3	channel
190	sm-72	5 ± 1	0 ± 2	channel
191	sm-60	25 ± 5	-15 ± 5	tire track
192	sm-61	0 ± 2	-3 ± 1	tire track
193	sm-119	5 ± 1	0 ± 1	small pull-apart
194	sm-71	10 ± 3	0	channel
195	sm-70		-12 ± 3	
197	sm-144	0 ± 5	20 ± 5T	tire track
198	sm-68		-30 ± 5	
199	sm-142	0 ± 10	35 ± 5	channel
200	sm-94	15 ± 5	-30 ± 5	tire track
201	sm-145	0 ± 10	-12 ± 1	channel
202	sm-67	0 ± 5	8 ± 5	channel
203	sm-62	0 ± 5	-5 ± 3	channel
204	sm-131		-15 ± 5	
205	sm-66	0 ± 5	-15 ± 3	channel
206	sm-93	30 ± 10	-10 ± 5	tire track
207	sm-22	0 ± 10	-10 ± 5	channel
209	sm-86		-20 ± 5 T	
210	sm-136	5 ± 1	0 ± 2	channel
211	sm-125	30 ± 5	0 ± 5	channel
212	sm-141	2 ± 1	5 ± 1	channel
213	sm-63	0 ± 5	-15 ± 3	channel
214	sm-140	0 ± 30	7	
215	sm-64	4 ± 2		
216	sm-134	-12 ± 3	-5 ± 3	tire track
217	sm-118	0 ± 3	-7 ± 1	channel
218	sm-135	18 ± 3	-8 ± 8	channel
219	sm-92	25 ± 10	-20 ± 5	tire track
220	sm-139	0 ± 5	11 ± 1	
221	sm-127		-30 ± 5	
222	sm-21	25 ± 10	-15 ± 5	double tire track
223	sm-133	20 ± 5	8 ± 1	tire track
224	sm-138	0 ± 5	-11 ± 1	
225	sm-17	30 ± 10	-20 ± 5	channel
226	sm-132	-15 ± 5	-20 ± 1 T	channel
227	sm-126	20 ± 5	-3 ± 1	channel
228	sm-20	10 ± 5	-15 ± 5	channel
229	sm-146			tension crack, 20 cm wide
230	sm-16	20 ± 5	-10 ± 5	channel
231	sm-147			tension crack, 20 cm wide
232	sm-19	15 ± 15	-10 ± 5	channel
233	sm-18	20 ± 10	0 ± 3	channel
234	sm-117	15 ± 3	0 ± 3	channel
235	sm-15	30 ± 10	-5 ± 5	gully

Table 2. (Continued)

Site		Right Lateral	Vertical	
Plate 1	Field Notes	Slip, cm	Slip,[a] cm	Description
236	sm-24	4 ± 1	0 ± 3	
237	sm-14	20 ± 10	0 ± 5	gully
238	cr-9			9.5-m-long, old shutter ridge
239	sm-9	4 ± 1		small pull-apart
240	sm-26	15 ± 5	-3 ± 2	ridge in dirt road
241	sm-25	2 ± 1	-2 ± 1	small pull-aparts
242	sm-23	2 ± 1	-3 ± 0	channel
243	sm-13	0 ± 10	0 ± 5	channel
244	sm-12	15 ± 15	0 ± 5	channel
245	cr-48	1		channel
246	sm-28	7 ± 2	-3 ± 1	channel
247	sm-27	2 ± 2	0 ± 2	channel
248	sm-29	5 ± 1	-1 ± 1	bar in channel
249	sm-8	25 ± 5	-10 ± 5	gully
250	sm-7	25 ± 5	-15 ± 5	channel
251	sm-11	25 ± 5	0 ± 5	channel
252	sm-10	35 ± 3	-10 ± 5	channel
253	sm-5	10 ± 10		channel
254	sm-30	50 ± 15	-17 ± 2	channel
255	sm-87	75 ± 10	-15 ± 10	channel
256	sm-88	42 ± 8	-8 ± 5	channel
257	sm-89	60 ± 10	12 ± 5	channel
258	sm-91	30 ± 15	-8 ± 5	channel
259	sm-115		-7	
260	sm-114	45 ± 25	-30 ± 5	channel and tire track
261	sm-113	10 ± 5	-11 ± 3	ridge between tire tracks
262	cr-14	20	5	channel
263	cr-45	20 ± 2	8 ± 1	channel
264	cr-46		12	
265	sm-99a	10 ± 3	-6 ± 3	
266	sm-99b	3 ± 1	0 ± 2	
267	sm-99c	0 ± 3	-8 ± 3	
268	sm-99d	1 ± 1	-12 ± 3	
269	cr-47	10 ± 1		tire track
270	sm-112			tension fissure, 10 cm wide
271	sm-101	12 ± 3	-25 ± 5	tire track
272	sm-107		-30 ± 5	
273	sm-108	0 ± 10	-40 ± 10	tire track
274	sm-109			tension fissures, 10 cm wide
275	sm-110	0 ± 2	-20 ± 5	tire tracks
276	sm-111	0 ± 3	-6 ± 2	tire track
277	cr-43	≥ 12	-15	
278	cr-42	14 ± 2	-16 ± 4	tire track
279	cr-41		-30	
280	cr-40	15	-34	tire track
281	cr-39	20	-18	
282	cr-20(2)	≥20	-19	
283	jz-73	35 ± 5		
284a	jz-34a	43 ± 10	0	
284b	jz-34b	11 ± 3	0	
284c	jz-34c	13 ± 3	-2	
284d	jz-34d	36 ± 5	0	
284e	jz-34e	33 ± 5		
285	jz-74	2 ± 0	9 ± 1	
286	jz-35		13 ± 3	
287	jz-36	30 ± 5		
288	cr-29	21		tire track
289	cr-28a	3.5		

[a] Positive values are east-side-up.
[b] *T* denotes thrust fault.

larly durable, and striations were preserved on the fault surface (Figure 2b). The best preserved striations were on an overhanging fault surface near site 19 with a strike of N68°W and a dip of 82°NE. This portion of the fault is within a compressional bend, and the displacement on the main fault trace had both a right-lateral and a reverse component. Five measurements of the plunge of the striations preserved on the fault surface on the northeastern side of the fault averaged 24°NW. This average plunge suggests a ratio of right-lateral to vertical slip of 2.25. This is nearly identical to the ratio of 2.23 found at the nearest slip measurement (site 19).

Along a ≥250-m length of the rupture, located 2.3 to 2.7 km southeast of Galway Lake Road, there was no brittle deformation at the surface (Plate 1). Rather, the ground surface was vertically warped, with the northeast side uplifted 30-70 cm. Ephemeral channels on the fan surface were right-laterally warped about 220-375 cm across this zone (Figure 2e).

3.4. Secondary Fractures

There were many secondary fractures away from the main fault zone, which exhibited substantial amounts (several tens of centimeters) of right-lateral, left-lateral, or thrust displacement (Table 2 and Figure 5). Other fractures exhibited only tensional opening. The orientation of the fractures with different senses of slip fit a simple strain ellipse defined by right-lateral shear along a north-northwest striking shear zone. Right-lateral fractures strike north to northwest, left-lateral fractures strike northeast, and thrust fractures strike west to northwest (Figure 6). We speculate that the fractures east of the main fault and near the northern end of our map area represent an attempted slip transfer from the Emerson fault to the Camp Rock fault to the east. The slip transfer failed, and the Emerson fault continued to carry the bulk of the right-lateral slip for 15 km farther north before finally stepping over completely to the Camp Rock fault. Secondary fractures on the west side of the fault, near the southern end of our map area, result from the transfer of slip from the Homestead Valley fault onto the Emerson fault [*Zachariasen and Sieh*, 1995].

4. Evidence for Prehistoric Earthquakes on the Emerson Fault

There is considerable geomorphic evidence for prehistoric movement on this portion of the Emerson fault, and several investigators have used this geomorphic evidence to estimate the timing and frequency of prehistoric earthquakes on this part of the fault [*Bull*, 1996; *Aydin et al.*, 1992; *Aydin and Du*, 1995; *Arrowsmith and Rhodes*, 1994]. These researchers generally agree that the most recent prehistoric earthquake on this part of the fault occurred at least several thousand years ago. In a trench across the fault near the southern end of our map area, *Rubin and Sieh* [1997] demonstrated that the most recent faulting event at that location occurred about 9000 years ago. *Bull* [1996] concurs that the most recent prehistoric earthquake at the southern end of our map area occurred in the early Holocene, but he also presents geomorphic evidence for a more recent prehistoric rupture (at $3 \pm {}^{2}_{1}$ ka) extending northwestward along the fault from near the pull-apart basin at our site 39.

4.1. Uplifted, Older Alluvial Fan Surfaces

Geomorphic evidence for prehistoric earthquakes can be found in the remnants of older alluvial fan surfaces that have been uplifted and preserved on the east side of the fault (see shaded areas in Plate 1 between sites 31 and 60 and in Figure

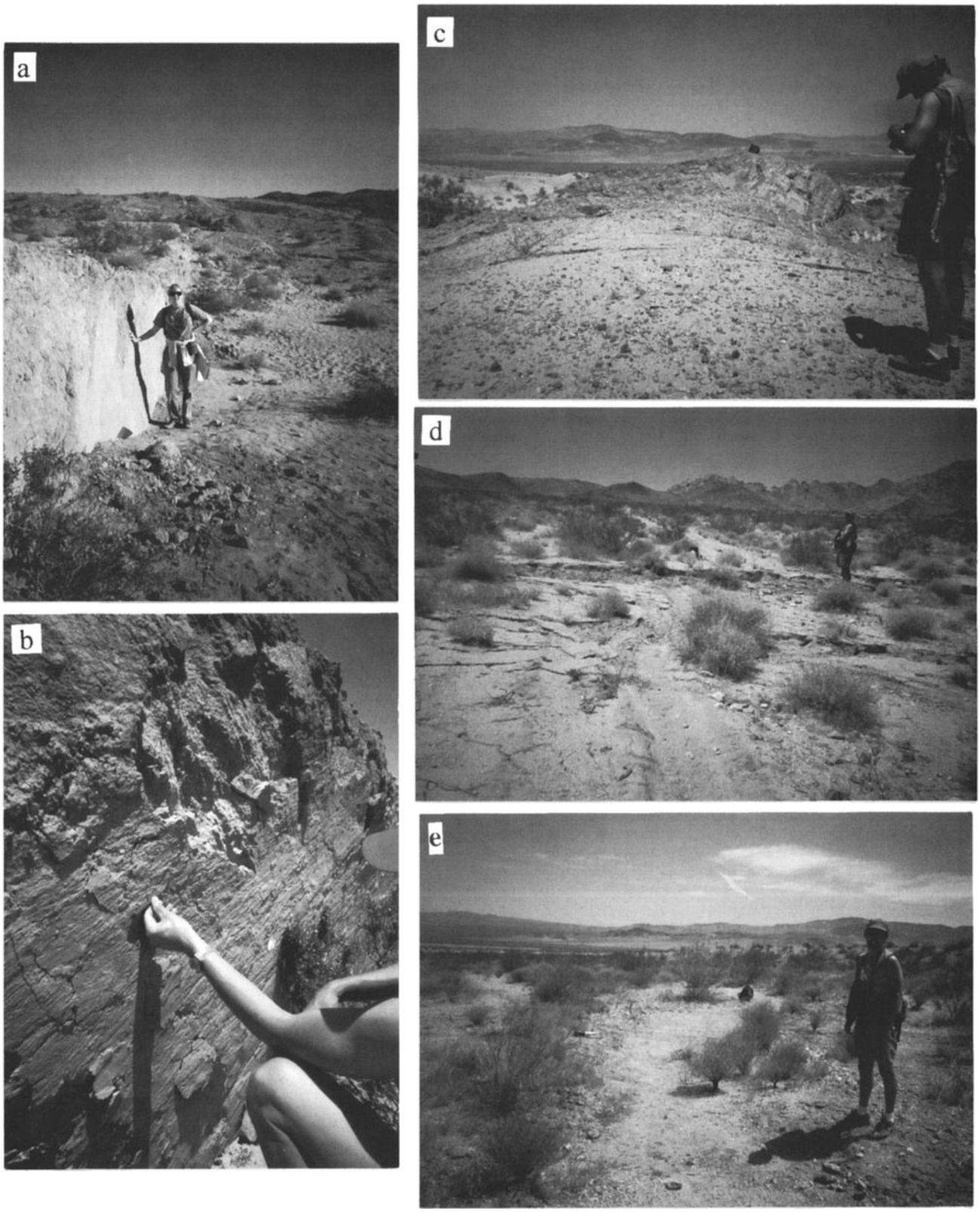

Figure 2. Photos of lateral and vertical displacements along the main fault rupture. Locations of numbered sites are shown on Plate 1. (a) A 186-cm-high fault scarp about 10 m southeast of site 18. Part of the vertical separation here is due to lateral offset of sloping topography. View is to southeast. (b) Exposed fault surface with striations, between sites 18 and 19. View is to northeast. (c) Ridge offset about 335 cm right laterally at site 19. View is to northeast. (d) Off-road vehicle track at site 41 offset 100 cm on fault trace in foreground, 323 cm on fault trace in background (where person is standing), and 10 cm on a minor fracture still farther in the background. View is to southwest. (e) Ephemeral channel warped 375 $\pm$ 35 cm right laterally and 70 cm east-side up at site 35. View is to northeast.

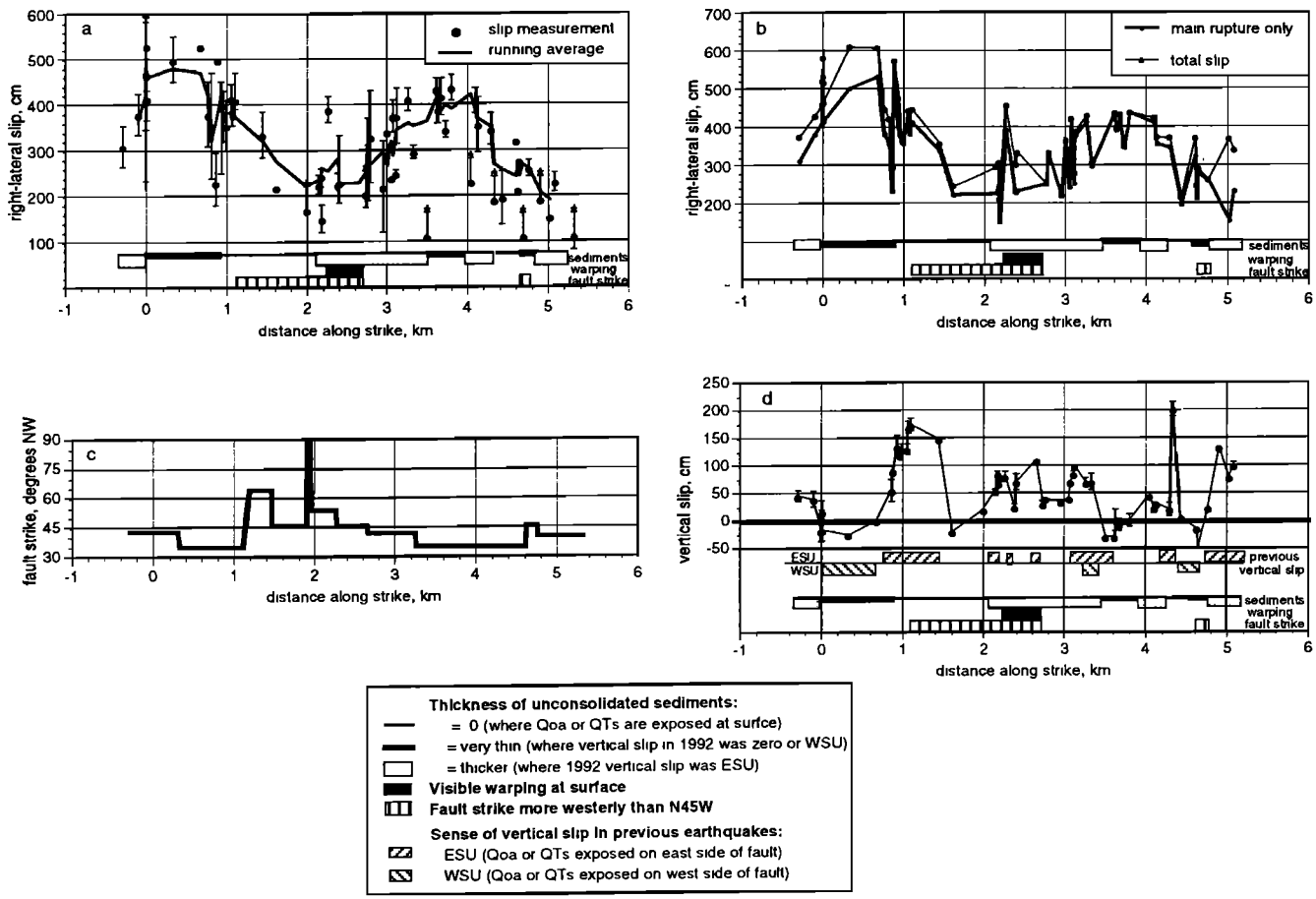

Figure 3. (a) Right-lateral slip as a function of distance along strike. Measurements shown here include slip on all fractures within a zone several tens of meters wide and centered on the main fault trace. Measurements that do not span the entire width of this zone are regarded as minimum values and are shown with triangles at the upper ends of the error bars. The solid line is a running average over three points, excluding minimum values. Horizontal bars at base of plot show inferred thickness of unconsolidated sediments as a function of distance along strike, the location of visible warping at the surface (see Plate 1 and Figure 6), and the locations in which the fault strikes more westerly than 45° NW. (b) Right-lateral slip versus distance along fault strike for the main fault rupture (heavy line) and with slip on secondary faults included (thinner line). Error bars are omitted for clarity. Horizontal bars at base of plot are as in Figure 3a. (c) Fault strike (azimuth) as a function of distance along strike. (d) Vertical slip on the main fault zone as a function of distance along fault strike. East-side-up (ESU) displacement is shown as positive vertical slip. The uppermost horizontal bars at base of plot show the sense of vertical slip in prehistoric earthquakes, as inferred from the locations of uplifted older alluvium (Qoa) and Plio-Pleistocene sediments (QTs). Lower horizontal bars are as in Figure 3a. In Figures 3a-3d, distance is measured southeastward from Galway Lake Road.

6 from 2.1 to 5.2 km southeast of Galway Lake Road). The southwestern edges of these older fan surfaces are located about 25 m northeast of (downstream from) the main 1992 rupture, and most likely are old fault scarps that have retreated away from the actual fault location by fluvial erosion. Two surveyed profiles (one just southeast of site 37 and the other just southeast of site 31) indicate that the scarps in these two surface remnants are 2 and 5 times higher, respectively, than the ~70-cm-high 1992 fault scarps in the same areas. The correlative surfaces west of the fault have been buried by Holocene alluvium, however, so the present height of the scarps in the older alluvium is a minimum estimate of the vertical displacement of those surfaces. This suggests that at least two to five earthquakes with a vertical slip distribution similar to the 1992 event would be required to produce these older scarps.

Bull [1996] regards the two uplifted surfaces described above as Pleistocene in age, most likely correlating with a regional aggradational event that occurred about 125 ka. If this is true and if the average recurrence interval for faulting events is comparable to the 9-kyr interval between the two most recent events [*Rubin and Sieh*, 1997], one would expect the scarps in the late Pleistocene surface to have formed as a result of about 13 earthquakes. This suggest that either (1) a substantial fraction of the scarps in the late Pleistocene alluvium has been buried by recent alluvium so that the portion of the older scarps that is visible represents only 15-40% of the total scarp height and/or (2) vertical slip in many of the prehistoric earthquakes was less than in 1992. *Rubin and Sieh* [1997] demonstrate that at the location of their trench site, vertical slip in the 9 ka event was similar to the vertical slip in 1992, which argues against the latter option.

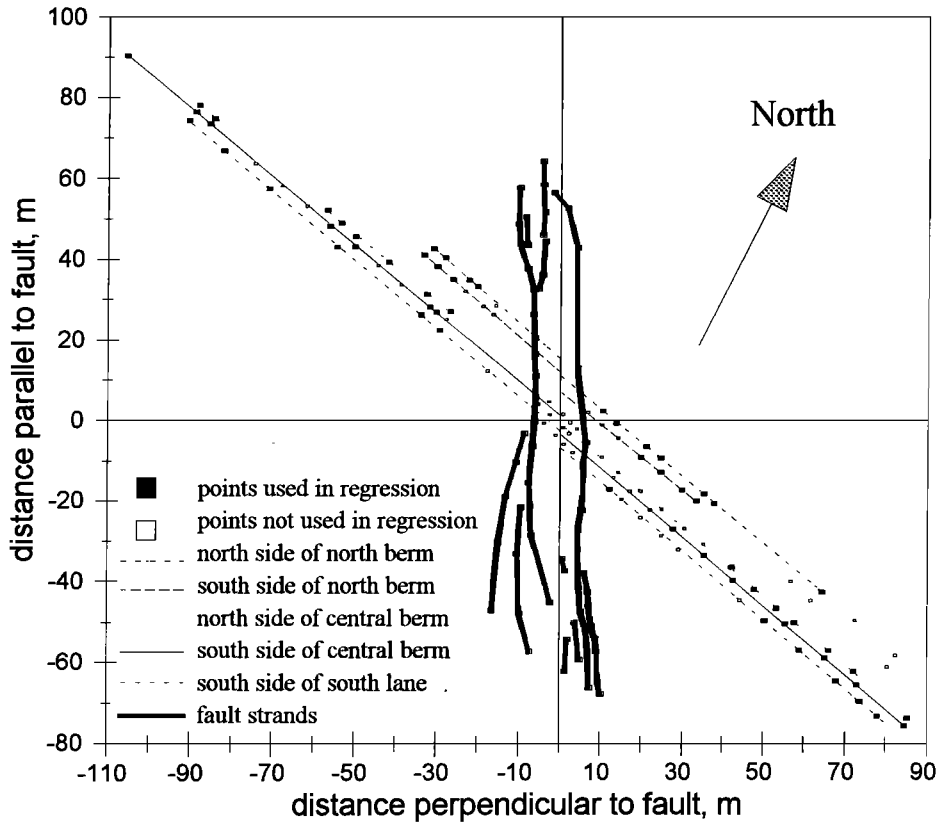

Figure 4. Map of offsets at Galway Lake Road surveyed on August 19, 1994. Some surveyed points along the road were not used in the regressions for one or more of the following reasons: (1) field notes indicated that the road edge or berm was poorly defined at that location, (2) points near the fault zone that appeared to have been influenced by lateral warping, or (3) far-field points that appeared to have a different trend than those at intermediate distances from the fault. At the time of the survey the south edge of the south lane was poorly defined on the west side of the fault. These points were used in the regression despite their uncertain quality because of the unavailability of better data. The detailed fracture pattern of the fault zone was not surveyed. Only the major bounding faults and selected minor faults are shown.

4.2. Uplifted Plio-Pleistocene Sediments

Additional geomorphic evidence for prehistoric earthquakes can be found where a small hill composed of Plio-Pleistocene sandstone [*Dibblee*, 1964] has been uplifted on the northeastern side of a left step (compressional fault jog) in the main fault zone (between sites 18 and 20 on Plate 1). This hill is bounded on the northeast by secondary thrust faults that ruptured in 1992 with a few tens of cm of vertical displacement (e.g., sites 173, 174, 180, 185, 187, 191, and 213) and on the southwest by the section of the main 1992 rupture zone that had the largest vertical displacements (sites 13 to 19). This hill was undoubtably uplifted by repeated earthquakes on this portion of the Emerson fault. *Aydin and Du* [1995] present a detailed structural analysis of this hill and of the 1992 rupture in this area.

Although the southwest side of the hill was uplifted 120-175 cm along the main rupture during the 1992 earthquake, the north side of the hill was only uplifted 5-15 cm in the west and 15-30 cm in the east along minor thrust faults. This

Table 3. Offset Measurements at Galway Lake Road

	Right-Lateral Offset, m		
	This Study[a]	U.S. Geological Survey[b]	Sieh, Hudnut, and Rubin[c]
North side of north berm	4.09 ± 1.75		
South side of north berm	4.71 ± 1.25	5.13 ± 0.17	6.35
North side of central berm	5.31 ± 0.62	5.27 ± 0.12	
South side of central berm	4.66 ± 0.35	5.15 ± 0.13	5.70[d]
South side of south lane	4.14 ± 0.47	5.24 ± 0.07	6.77

[a] Linear regressions of surveyed points. Stated uncertainties are ±1 σ and were calculated from the 95% confidence interval on the *y* intercept of the regression lines.
[b] Linear regressions of surveyed points. Stated uncertainties are ± the standard error in the *y* intercept. Data are from D. Ponti (personal communication, 1993).
[c] Measurement with steel tape. Data are from unpublished field notes of K. Sieh.
[d] Crest of central berm.

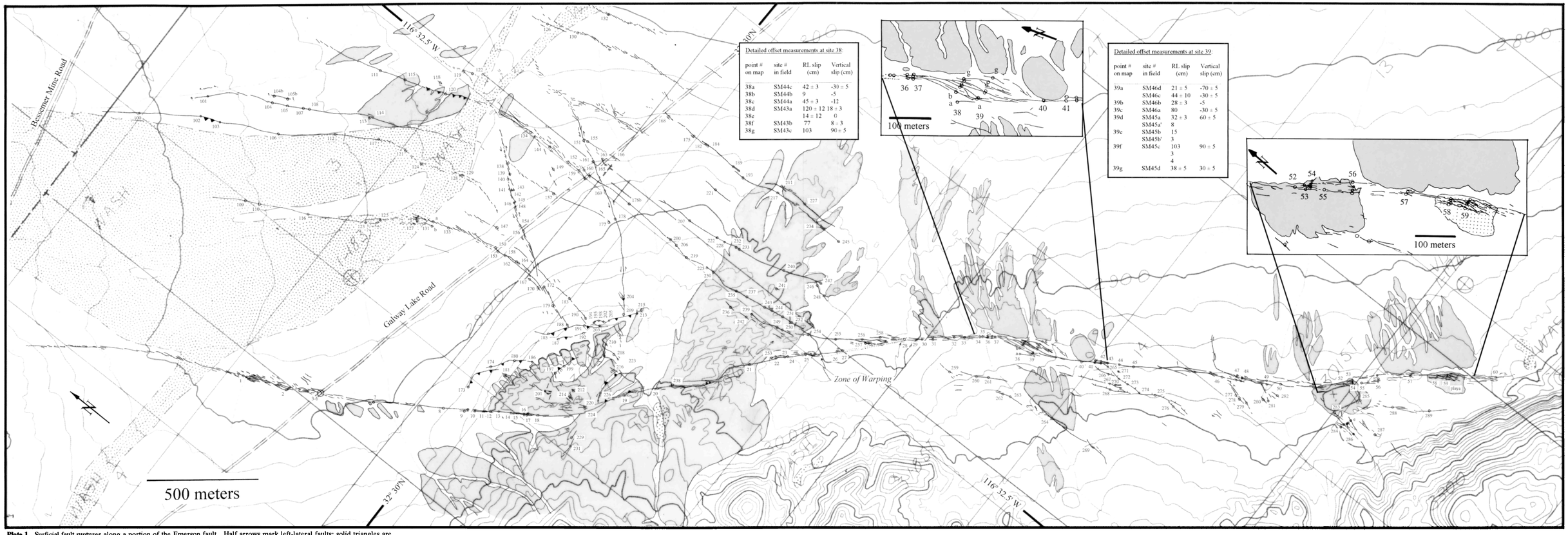

Detailed offset measurements at site 38:

point # on map	site # in field	RL slip (cm)	Vertical slip (cm)
38a	SM44c	42 ± 3	-30 ± 5
38b	SM44b	9	-5
38c	SM44a	45 ± 3	-12
38d	SM43a	120 ± 12	18 ± 3
38e		14 ± 12	0
38f	SM43b	77	8 ± 3
38g	SM43c	103	90 ± 5

Detailed offset measurements at site 39:

point # on map	site # in field	RL slip (cm)	Vertical slip (cm)
39a	SM46d	21 ± 5	-70 ± 5
	SM46c	44 ± 10	-30 ± 5
39b	SM46b	28 ± 3	-5
39c	SM46a	80	-30 ± 5
39d	SM45a	32 ± 3	60 ± 5
	SM45a'	8	
39e	SM45b	15	
	SM45b'	3	
39f	SM45c	103	90 ± 5
		3	
		4	
39g	SM45d	38 ± 5	30 ± 5

Plate 1. Surficial fault ruptures along a portion of the Emerson fault. Half arrows mark left-lateral faults; solid triangles are on the upper plate of thrust faults; hachures are on the downthrown side of vertical faults with primarily vertical displacement; all other faults are right lateral. Dotted lines show areas where ground surface was visibly warped, both horizontally and vertically, but where brittle fractures were limited or absent. Numbered open circles mark the locations of slip measurements listed in Tables 1 and 2. Shaded areas are uplifted, older alluvial fan surfaces and Plio-Pleistocene sediments. Topographic base is from the U.S. Geological Survey, Iron Ridge 7.5 arc min quadrangle. Contour interval is 6.1 m (20 feet).

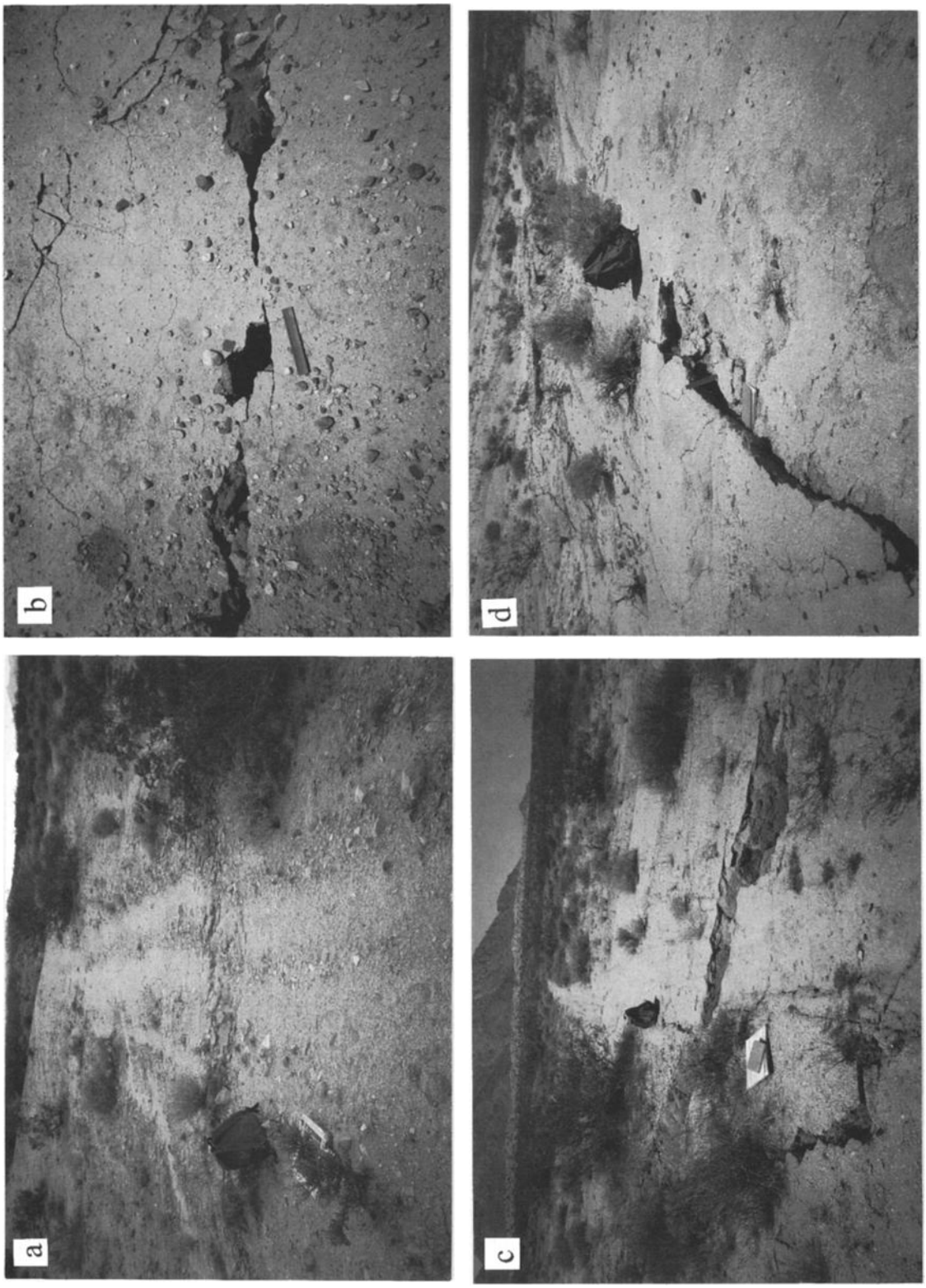

Figure 5. Photos of secondary faults. Locations of sites are shown on Plate 1. (a) Pebble alignment between two sandy tire tracks offset 25 ± 10 cm right laterally at site 222. View is to southwest. (b) Small pull-apart cavity. Matching the two sides of the pull-apart indicates 10 cm of right-lateral slip on this crack. Ruler is 15 cm long. (c) Off-road vehicle track offset 50 ± 5 cm left laterally along a secondary fracture at site 169. View is to northwest. (d) Secondary fault with about 15 cm of reverse displacement. A few meters away, at site 226, a channel is offset 15 ± 5 cm left laterally along the same fracture. View is to the east.

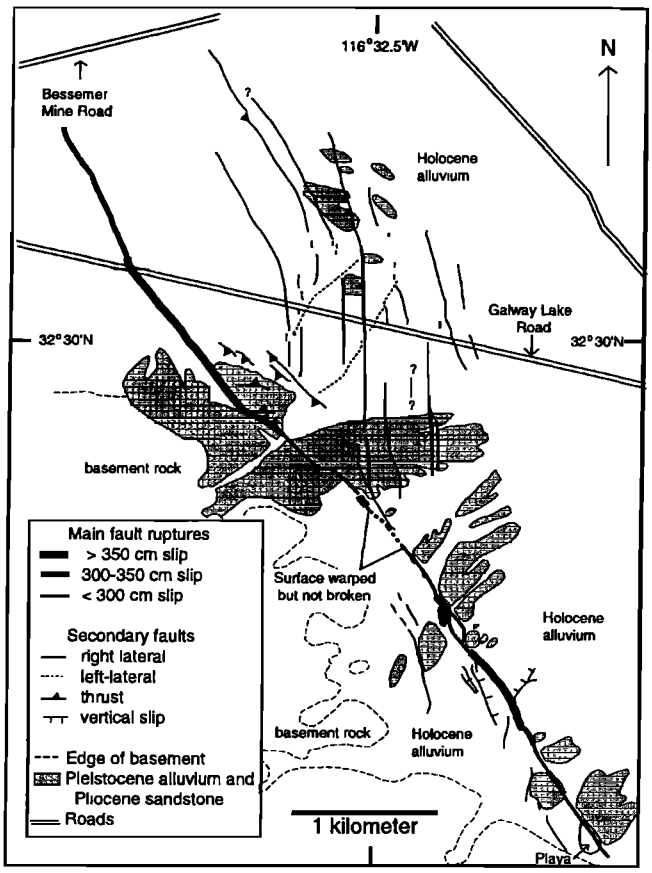

Figure 6. Simplified map of fault ruptures that illustrates the orientations of fractures with different senses of slip as well as the locations of high- and low-slip areas along the main rupture.

suggests that the hill was tilted down to the northeast by 0.15° to 0.38° during the 1992 earthquake. The Plio-Pleistocene sandstone that forms the hill dips 25° to 45° northeastward [*Dibblee*, 1964] suggesting a long history of deformation, associated with many prehistoric earthquakes. In particular, these data suggest that a few hundred earthquakes with deformation comparable to that in the 1992 event may be responsible for the current dip of the sandstone beds. A volcanic ash near the base of the sandstone has been chemically correlated with the 3.4 Ma Nomlaki Tuff [*Aydin et al.*, 1992]. This suggests that the average interval between earthquakes has been a few tens of thousands of years. Given the uncertainties involved, this estimate is roughly consistent with the 9-kyr interval between the two most recent events documented by *Rubin and Sieh* [1997].

4.3. Timing of the Most Recent Prehistoric Earthquake

Bull [1996] concurs with *Rubin and Sieh* [1997] that the most recent prehistoric earthquake at the southern end of our map area occurred in the early Holocene, but he also presents evidence for a more recent prehistoric rupture (at $3 \pm {}^{2}_{1}$ ka) extending northwestward along the fault from near the pull-apart basin at our site 39. In the area between our sites 22 and 25, a late Holocene surface (not shown in Plate 1) is truncated sharply at the 1992 rupture and is juxtaposed against modern alluvium on the west side of the rupture [*Bull*, 1996, Figure 9]. These observations suggest the possibility of a pre-1992 (but post-9 ka) earthquake that uplifted the late Holocene surface on the east side of the fault and ponded younger sediments on the west behind an uphill-facing scarp. In support of this, a small channel within the late Holocene deposits parallels the fault for a short distance and may have been deflected by an uphill-facing scarp [*Bull*, 1996]. Isolated patches of late Holocene alluvium are present on the west side of the fault, however (*Bull* [1996] and our own observations). After restoring the vertical slip represented by the 1992 fault scarp, any preexisting scarp would have to have been small.

In one location, *Bull* [1996] observed a slight bevel at the crest of the 1992 scarp, which may be a remnant of a pre-1992 scarp in the late Holocene alluvium. In much of this area, however, the pavement of the late Holocene surface is truncated sharply by the 1992 rupture plane, with no visible remnants of an older, more subdued scarp. The interpretation of the fan deposits in the vicinity of sites 22 to 25 remains somewhat ambiguous, but *Bull's* [1996] hypothesis of a late Holocene earthquake at this location appears to be the most reasonable interpretation.

It is worth noting that *Arrowsmith and Rhodes's* [1994] modeling of scarp degradation suggests that more than 10 kyr would be required to reduce the 1992 fault scarp at our site 18 to its pre-1992 form. This contradicts *Bull's* [1996] hypothesis of a late Holocene rupture on the northern Emerson fault. However, the scarp modeling could perhaps be reconciled with the geomorphic evidence for a late Holocene earthquake if that earthquake produced less vertical slip than the 1992 earthquake.

4.4. Right-Lateral Slip in Prehistoric Earthquakes

Very little evidence for lateral slip in previous earthquakes was preserved. A 9.5-m-long shutter ridge at site 238 is the only feature we found that may preserve the lateral offset in the most recent few prehistoric earthquakes on the Emerson fault. A few other features suggest repeated right-lateral slip over a longer time period. For example, a channel incised into the uplifted, older alluvial fan surface in the vicinity of site 21 has a right bend of about 120-150 m at the location of the 1992 rupture (Plate 1). *Aydin and Du* [1995] propose additional correlations of channels and an old alluvial fan edge across the fault that suggest a prior history of right-lateral slip.

5. Variability of Surficial Slip

Variability in lateral slip along the main fault zone occurs at both large and small length scales (Figures 3a and 3b). Relatively large offsets (about 4 m) occurred along the main trace between 0 and 1.5 km south of Galway Lake Road and between about 3.1 and 4.2 km south of Galway Lake Road. Smaller displacements (about 2 m) occurred between 1.5 and 3.1 km and between 4.2 and 5.2 km south of Galway Lake Road.

Superimposed on these kilometer-scale variations in slip are variations that occur over distances of several tens of meters, which produce the spikiness in the slip distribution (Figure 3b). Even over distances < 1 km, slip occasionally varies by a factor of 2, and in several places the slip across the main trace varies by 1 m or more within a few tens of meters along the strike of the fault. The slip gradient may be

Table 4. Most Extreme Slip Gradients Along the Central Emerson and Garlock Faults

Measurement Pair	Offset 1, m	Offset 2, m	Δ Offset, m		Δ Distance m	Slip Gradient	
			Preferred	Minimum		Preferred	Minimum
			Emerson Fault: Galway Lake Road				
5/6 (SM248 / SM247)[a]	4.66 ± 0.35	4.14 ± 0.47	0.52	0	4	0.13	0
4/5 (SM249 / SM248)[a]	5.31 ± 0.62	4.66 ± 0.35	0.65	0	3	0.22	0
3/4 (SM250 / SM 249)[a]	4.71 ± 1.25	5.31 ± 0.62	0.60	0	7	0.09	0
3a/3 (SM251 / SM250)[a]	4.09 ± 1.75	4.71 ± 1.25	0.62	0	3	0.21	0
			Emerson Fault: Other Locations				
36/37 (SM41 / SM42)[a]	$2.2 \pm {}^{0.50}_{0.75}$	3.75 ± 0.6	$1.55 \pm {}^{0.96}_{0.78}$	0.77	18	0.09	0.04
34/35 (SM39 / SM40)	2.4 ± 0.6	3.75 ± 0.35	1.35 ± 0.69	0.66	12	0.11	0.06
23/24 (SM4 / SM32)	2.45 ± 0.3	1.5 ± 0.3	0.95 ± 0.42	0.53	11	0.09	0.05
			Garlock Fault[b]				
2-63(3) / 2-63(2)	8.8 ± 0.7	$2.5 \pm {}^{1.7}_{0.7}$	6.3	3.9	6	1.05	0.65
2-61(6) / 2-61(7)	5.3 ± 0.3	3.4 ± 0.5	1.9	1.1	4	0.48	0.28
2-33(5) / 2-33(6)	8.4 ± 1.6	2.4 ± 0.5	6.0	3.9	20	0.3	0.2
2-61(5) / 2-61(4)	5.6 ± 0.7	2.7 ± 0.7	2.9	1.5	10	0.29	0.15
2-63(3) / 2-63(5a)	8.8 ± 0.7	$2.3 \pm {}^{2.0}_{0.5}$	6.5	3.8	25	0.26	0.15

[a] Surveyed measurement.
[b] From *McGill and Sieh* [1991].

used to quantify these short-wavelength variations in slip. The slip gradient is the difference in lateral slip between any two offset features divided by the distance along the fault between the two features and is also equivalent to the compressional (or extensional) strain parallel to the fault. The median slip gradient for the portion of the fault that we mapped was about 10^{-3} and the largest slip gradients were close to 10^{-1}. When the slip gradient is calculated using the preferred offset measurements, seven pairs of lateral slip measurements on the main fault trace had slip gradients close to 10^{-1} (Table 4). When the slip gradient is calculated using the extreme ends of the error bars on the slip measurements, so as to minimize the slip gradient, then most of these slip gradients are reduced to 10^{-2} or less.

Surficial slip gradients as large as 10^{-1} have not been reported previously. The maximum slip gradients on other faults that ruptured during the Landers earthquake were of the order of 10^{-2}, using the preferred slip values for measurements contributed by other geologists to the Southern California Earthquake Center (SCEC) database. The maximum slip gradients calculated from published data on other historical strike-slip ruptures is also 10^{-2} [*Williams and Magistrale*, 1989; *Sharp et al.*, 1982; *Ambraseys and Tchalenko*, 1969]. The fact that the slip gradients along the Emerson fault are slightly more extreme than elsewhere along the Landers rupture and than along other historical ruptures may reflect the high density of off-road vehicle tracks and other linear features that allowed very closely spaced lateral offset measurements to be made.

5.1. Measurement Error

Before discussing possible explanations for the observed variations in surficial slip, it is important to consider whether the observed slip variations are real or whether they may be the result of measurement errors. We measured the offsets of four of the features discussed here independently on different occasions. In addition, *Irvine and Hill* [1993] and K. Sieh (personal communication, 1998) made slip measurements on some of the same features that we measured. Although there is some uncertainty in determining which of our measurements correspond to the measurements published by *Irvine and Hill* [1993], in most cases the mapped location of the measurement and the description of the offset feature (e.g., stream channel versus off-road vehicle track) are sufficient to determine the correspondence with reasonable certainty. The difference between independent measurements on 13 features ranges from -160 cm to 115 cm, and the average of the absolute values of the differences is 49 cm (Table 5).

As an example, an extreme slip gradient between a pair of offset channels is documented in Figure 7. The lateral offsets measured from the surveyed map differ from the taped field measurements for both channels, and the difference is significant for one of them. Comparison of the surveyed offset at site 37 with the taped measurement suggests that the errors in some measurements may be as large as 160 cm (30%). The taped measurements for features 36 and 37 had indicated a preferred slip gradient of 0.17 and a minimum slip gradient of 0.11. The surveyed measurements indicate that measurement error is partly responsible for the large slip gradient, but they still yield a preferred slip gradient of 0.09 and a minimum slip gradient of 0.04 (Table 4). Thus, in at least one location along the Landers rupture, surveyed measurements indicate that the slip gradient was at least 10^{-2} and possibly close to 10^{-1}.

While the slip variations of up to 160 cm between individual measurements may be due to measurement error in some cases, to explain the kilometer-scale variations in slip as measurement error would require that we consistently overestimated the slip along some fault sections and consistently underestimated it along other sections. This seems unlikely.

5.2. Secondary Fractures

The variations in slip (at both short and long length scales) are not artifacts of comparing slip across the entire width of the main fault zone at one point with the slip across a portion of the fault zone at another point. As mentioned previously, we were quite careful to measure the lateral slip across every visible fracture within a zone several tens of meters wide centered on the main fault zone and to include all of the slip

Table 5. Summary of Independent Measurements of Fault Slip at the Same Location

		Measurement 1				Measurement 2			
Site (Plate 1)	Difference in Slip, cm	Site (Field Notes)	Right-Lateral Slip, cm	Observer(s)	Method	Site (Field Notes)	Right-Lateral Slip, cm	Observer(s)	Method
18[a]	33	CR6	392	Rubin and McGill	steel tape	SM81	$425 \pm \frac{45}{29}$	McGill and Slates	steel tape
23[a]	30	SM4	230 ± 27	McGill	steel tape	SM4	260	McGill and Rubin	steel tape
25[a]	-75	CR11	425 ± 25	Rubin and McGill	steel tape	SM33	350 ± 20	McGill and Rubin	steel tape
48[a]	-53	CR19	380	Rubin and McGill	steel tape	SM104	327 ± 30	McGill and Rubin	steel tape
16?[b]	35	SM79	415 ± 30	McGill and Slates	steel tape	1	450	*Irvine and Hill* [1993]	unknown
43?[b]	-27	SM99	417 ± 40	McGill and Rubin	steel tape	2	390	*Irvine and Hill* [1993]	unknown
53?[b]	-46	CR34	211	Rubin and McGill	steel tape	6	165	*Irvine and Hill* [1993]	unknown
58?[b]	-27	CR26	152	Rubin and McGill	steel tape	8	125	*Irvine and Hill* [1993]	unknown
36	-30	SM41	250 ± 7	McGill and Rubin	steel tape	SM41	$220 \pm \frac{50}{70}$	McGill	surveyed
37	-160	SM42	535 ± 80	McGill and Rubin	steel tape	SM42	375 ± 60	McGill	surveyed
41	-0.5	CR16	433 ± 25	Rubin and McGill	steel tape	"Northern"	415-450	K. Sieh	surveyed
44?	115	SM100	345 ± 18	McGill and Rubin	steel tape	d, "Central"	460	K. Sieh	surveyed
45	-6	SM102	436 ± 26	McGill and Rubin	steel tape	f, "Southern"	430	K. Sieh	surveyed

[a] Value reported in Table 1 is the average of the two values reported here.
[b] In these cases it is less certain that the two sets of measurements were made on the same features.

within this zone in our estimate of the slip across the main fault zone.

The two, kilometer-long areas with smaller displacements on the main trace (1.5 to 3.1 and 4.2 to 5.2 km south of Galway Lake Road) partly coincide with areas in which many fractures are present away from the main trace (Figure 6). The right-lateral slip on these secondary fractures partially fills the slip deficit along some parts of the low-slip portions of the main trace but does not even come close to producing a uniform distribution of slip along strike (Figure 3b).

5.3. Slip on Visible Fractures Versus Total Shear

The variations in surficial slip (at both short and long length scales) represent real variations in the amount of brittle slip on visible fractures at the surface, but they do not necessarily indicate comparable variations in the total shear across the fault zone. As mentioned previously, a significant amount of lateral displacement may have occurred as warping (distributed shear), thus explaining why the offset of the line of transmission line towers across the northern Emerson fault was larger than the sum of the lateral slip on visible fractures

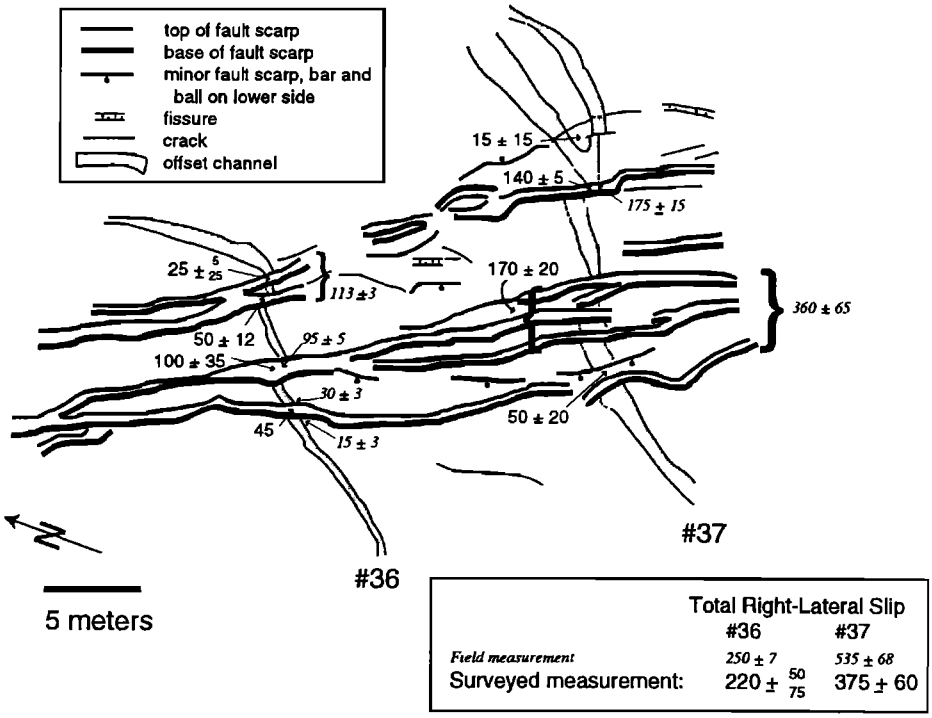

Figure 7. Surveyed map showing a pair of offset channels with one of the most extreme slip gradients, sites 36 and 37, on Plate 1 and Table 1. Nails were placed along the offset channels and fault strands on January 5, 1994 and the nails were surveyed on January 5 and August 18, 1994.

at that site [*Yeats et al.*, 1997]. Distributed shear is only measurable where a feature with known preearthquake geometry crosses the fault (e.g., the line of transmission line towers mentioned above, or the fence in Figure 5 of *Johnson et al.* [1994]). The variations in slip that we observed may represent variations in the proportion of the total shear that is concentrated onto visible fractures, rather variations in the total shear across the fault zone.

5.3.1. Short-wavelength example. In the example shown in Figure 7, we speculate that the measured slip at site 36 is lower than at site 37 because a larger proportion of the total surficial displacement across the fault zone at site 36 has occurred as either (1) distributed, brittle shear on fractures too small to be visible (e.g., between individual grains of sediment), (2) elastic or permanent warping of the uppermost sediments over brittle fractures that did not propagate all the way to the surface (as in work by *Bonilla and Lienkaemper* [1990]), or (3) clockwise rotation of small blocks, as documented by *Johnson et al.* [1994] elsewhere along the Landers rupture.

Any of these three mechanisms would produce either a real or apparent clockwise rotation of the portion of the channel at site 36 within the fault zone. The amount of rotation required to explain the missing slip at site 36 would be roughly equal to $\tan^{-1}(\Delta d/\lambda)$, where Δd is the amount of missing slip and λ is the cross-strike width of the fault zone. To explain the 1.55 m of missing slip at site 36 with one of the mechanisms above would imply that the channel has been rotated clockwise (either as a block or through distributed shear) by 6° to 10° over the 9- to 15-m width of the fault zone. Given the fact that the initial geometry of the channel is unknown, it seems quite possible that this amount of apparent rotation could have occurred without being noticeable. We do not know why a larger amount of unmeasurable shear may have occurred at site 36 than at site 37.

5.3.2. Application to long-wavelength variations. The same three mechanisms discussed above may also partially explain the kilometer-scale variations in slip. It seems reasonable to hypothesize that a larger proportion of the total displacement would be concentrated on visible fractures (and thus be measurable) in areas where the surficial materials are well consolidated than in areas where the surficial materials are unconsolidated. Thus one might expect the high slip areas to correlate with areas in which the surficial materials are well consolidated. To a certain extent, this is what we observe. Along the southern third of the high-slip area from 0 to 1.5 km, the fault ruptures through consolidated Pliocene or Pleistocene sandstone [*Dibblee*, 1964], whereas most of the remainder of the surface rupture is in unconsolidated, Holocene alluvium (Figure 6). However, this does not explain the areas of high slip between 0 and 0.8 km and between 3.1 and 4.2 km southeast of Galway Lake Road.

Perhaps these other high-slip areas are underlain by consolidated materials at very shallow depth, and the low-slip areas are areas in which the thickness of unconsolidated sediments is greater. In general, we suspect that the unconsolidated sediments along this portion of the Emerson fault are rather thin. *Dibblee* [1964] apparently shares this view. His cross sections show that he expects that the Holocene alluvium in this area is no more a few tens of meters thick and that the depth to crystalline basement rock (biotite quartz monzonite) is probably of the order of 100 m. A paleoseismic trench within the playa at the southern end of our map area reveals that the thickness of Holocene sediments is about 2.5 m at that location [*Rubin and Sieh*, 1997], but the underlying latest Pleistocene sediments were also relatively unconsolidated.

We have no direct information regarding how the thickness of unconsolidated sediments at the fault varies along the strike of the fault. However, we expect that this thickness is greater in areas where repeated, east-side-up vertical slip on the fault has produced an uphill-facing scarp, which ponded behind it young sediments from the eastward flowing drainages. As discussed above, the 1.7-m- to 3.8-m-high fault scarps in the Pleistocene alluvium at sites 37 and 31, respectively, may only represent 15% to 40% of the total scarp height. The correlative surface on the west side of the fault may be buried beneath 5-10 m of unconsolidated sediments.

The patterns at the bottom of Figures 3a and 3b show the inferred thickness of unconsolidated sediments at the fault as a function of distance along strike. The thickness of loose sediments is zero where consolidated materials (older alluvium or Plio-Pleistocene sandstone) are exposed at the surface. Where consolidated materials are not exposed at the surface, we assume that the veneer of loose sediments is very thin where the vertical slip in the 1992 earthquake was near zero or up on the west side and that the loose sediments are thicker where significant east-side-up vertical slip occurred in 1992. As mentioned previously, the locations in which Pleistocene alluvium has been uplifted on the east side of the fault, roughly coincide with the locations of large east-side-up vertical slip in 1992 (Figure 3d), suggesting that the pattern of vertical slip in the 1992 earthquake may be representative of the vertical slip in previous earthquakes.

From Figures 3a and 3b we can see that the two fault segments with lower right-lateral slip (1.5-3.1 km and 4.2-5.1 km) correspond in part to the fault segments along which the inferred thickness of loose sediments is greater. This suggests that variations in the depth to consolidated sediment or bedrock may partially explain the kilometer-scale variations in slip. However, if our inferences about the thickness of loose sediments are correct, then other factors must also be involved because there are low-slip areas where consolidated

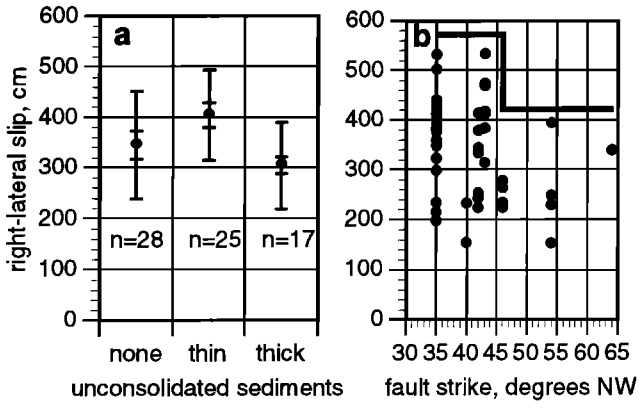

Figure 8. (a) Average of right-lateral slip measurements for areas with various inferred thickness of unconsolidated sediment. Broader error bars represent the standard deviation of the slip measurements, and narrower error bars represent the standard error of the mean. The number of measurements (n) included in each average is also shown. (b) Scatter plot of right-lateral slip versus fault strike.

sediments are exposed at the surface (e.g., at about 1.6 km and from 4.3 to 4.8 km southeast of Galway Lake Road) and high slip areas where the unconsolidated sediments are inferred to be relatively thick (e.g., from 3.1 to 3.5 km and from 4.0 to 4.3 km southeast of Galway Lake Road). Similarly, Figure 8a shows that there is not a strong correlation between right lateral slip and inferred relative thickness of unconsolidated sediments.

5.4. Other Possible Explanations for the Kilometer-Wavelength Variations in Slip

5.4.1. Complexities in the fault geometry. The low-slip segment from 1.5 to 3.1 km is bounded on the southeast by a 70-m-wide dilational step over and on the northwest by a 130-m-wide compressional fault bend (Figure 6). This is consistent with *Sibson's* [1986] observation that 100- to 1000-m-wide fault jogs are "commonly associated with abrupt changes in the amount of slip accompanying individual earthquakes [*Clark*, 1972; *Tchalenko and Berberian*, 1975; *Sieh*, 1978]". *Deng et al.* [1986] made a similar observation. This is also similar to the behavior observed in some numerical crack models. *Das and Aki* [1977] showed that when unbroken barriers remain on a fault plane, the slip on the fault is relatively uniform between any two barriers but that the slip on adjacent segments separated by barriers may be different. Furthermore, in the numerical models the slip on each segment is related to the length of the segment (see Das and Aki's Figure 4). If fault jogs act as barriers to slip and limit the effective, local rupture length to the distance between jogs, then one might expect the slip in an earthquake to change abruptly at fault jogs and to be lower on shorter fault segments. This mechanism can not explain all of the slip variability, however. The change from high slip north of 4.2 km to low slip south of 4.2 km does not coincide with any significant fault jog (Figures 3 and 6), and the 65-m-wide compressional fault bend at 1.9 km south of Galway Lake Road does not coincide with any marked change in right-lateral slip (Figures 3a and 3c).

5.4.2. Fault strike. There is a moderate correlation between the local strike of the fault and the amount of right-lateral slip. Figure 8b shows that the right-lateral slip on segments striking more westerly than N45°W is generally lower than on the more northerly striking segments. The patterns at the bottom of Figures 3a and 3b show the locations of fault segments with strikes more westerly than N45°W (data from Figure 3c). These segments correlate rather well with the low-slip segments, particularly with the central low-slip segment from 1.5 to 3.1 km. The more westerly trend of the fault in this low-slip segment represents a broad, gentle restraining bend (Figure 6). A similar pattern of lower slip in a broad, gentle restraining bend was observed in the 1968 Dasht-e Bayaz rupture (at chainage 2W to 2.5W in Figure 4 of *Ambrasseys and Tchalenko* [1969]). This mechanism does not explain most of the low-slip area from 4.2 to 5.2 km, however.

Restraining bends are areas in which one would expect the normal stress to be increased during an earthquake. This increase in normal stress would increase the dynamic friction shear stress on the fault. If the final stress on the fault after the earthquake is equal to the dynamic friction stress, then fault segments with higher dynamic friction stress will have a lower shear stress drop and slip (assuming uniform initial shear stress on the fault). However, this explanation is difficult to apply to repeated earthquakes because if slip is always lower on the more westerly trending segments then some sort of off-fault deformation must occur to compensate for the lower slip. As discussed above, the slip on the mapped secondary fractures is not sufficient to compensate for the areas of lower slip on the main fault.

5.4.3. Variations in slip in the previous earthquake. If the distribution of slip along strike in the previous earthquake was uneven, then the initial stress on the fault just prior to the 1992 event may have been unevenly distributed along strike. This in turn could result in variations in stress drop and slip in the 1992 event. If the slip on the fault is constant along strike when averaged over long time periods (i.e., over many earthquake cycles), then fault patches that have lower than average slip in one or more events must either have higher than average slip in other events, or they must fail more frequently than the high-slip patches. In principle, it should be possible to test the hypothesis that fault sections that had relatively high slip in 1992 had relatively low slip in the prior event by measuring the lateral offset of stream channels and other geomorphic features that were displaced in the pre-1992 event. Unfortunately, any geomorphic markers of the slip in the previous earthquake have been either destroyed by erosion or buried by younger sediment in the 9000 years that have elapsed since the prior event. While it seems intuitively obvious that variations in slip in the prior earthquake could produce variations in slip in the current event, this explanation begs the question of what caused variations in slip during the prior event.

5.5. Summary of Possible Causes of the Slip Variations

Some of the decameter-scale variations in slip may be at least partly attributed to measurement error, but others represent real variations in the amount of brittle slip on visible fractures at the surface. The kilometer-scale variations in slip can not be attributed to measurement error. Neither the short- or long-wavelength slip variations can be explained by slip on secondary fractures away from the main fault.

The decameter-scale variations in slip are most likely caused by incomplete expression of the slip within the surficial materials, either due to distributed brittle shear, to elastic or permanent lateral warping, or to rotations of small blocks within the fault zone. The kilometer-scale slip variations may be explained in part by these same factors, but they also appear to be related to the fault geometry in two ways: (1) the endpoints of the central low-slip segment coincide with fault jogs and (2) slip is lower on more westerly striking (convergent) fault segments, where the normal stress is probably higher. While other factors such as prior history of slip on the fault, material properties of the fault zone [*Revenaugh*, 1995; *Michael and Eberhart-Phillips*, 1991; *Lees and Nicholson*, 1993], and the dynamics of the rupture process [*Heaton*, 1990] may affect the distribution of slip on a fault, our observations do not directly bear on these factors, so we leave the exploration of these issues as a topic for future research.

5.6. Depth Extent of the Slip Variations

Modeling of geodetic observations and of seismic waves indicates that variation of slip on the fault plane also occurred at depth, with wavelengths of the order of 10 km [*Cohee and*

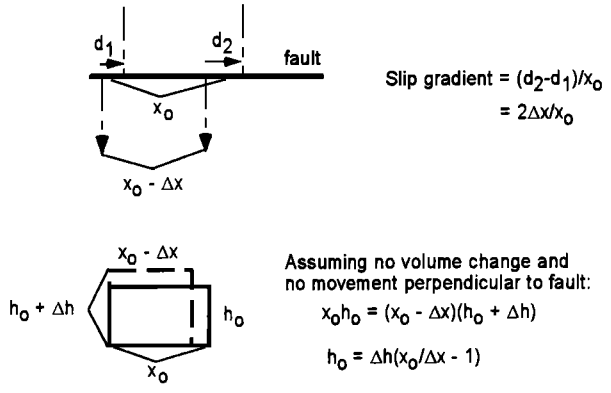

Examples:

Δh, m	2Δx/xo (slip gradient)	ho, m
0 5	0.09	10.6
3	0 002	2997

Figure 9. (top) Map view of two channels offset by amounts d_1 and d_2 across the fault. (middle) Cross section parallel to and on one side of the fault, and derivation of the relationship between the slip gradient ($2\Delta x/x_o$), the depth extent of the slip gradient (h_o), and the amount of local uplift (Δh). (bottom) Calculation of the depth extent of the slip gradient for two specific examples discussed in text.

Beroza, 1994; *Wald and Heaton*, 1994]. Whether or not the shorter-wavelength variations that we observe at the surface also exist on the fault at depth is not known, but we may make the following observations.

The variations in slip that we have observed are variations in the amount of slip on visible, brittle fractures. The total shear across the fault zone (S_T) is the sum of this measurable slip (S_M) and any unmeasurable shear (S_U) that may have occurred through distributed brittle slip, warping, or rotation. Intuitively, there is a limit to how deep any variations in the total shear (S_T) may extend. Variations in the total shear will produce compressional (or extensional) strain parallel to the fault zone ($(x_o - \Delta x) / x_o$; see Figure 9). Assuming that there is no movement of material perpendicular to the fault and that any volume changes are minimal, the fault-parallel compressional (or extensional) strain will be accompanied by a vertical extensional (or compressional) strain ($(h_o + \Delta h)/ h_o$).

The measured slip gradient between sites 36 and 37 is at least 0.04 and more likely 0.09 (Table 4). No anomalous uplift or subsidence was observed in this area. Any such local uplift or subsidence probably would have been noticeable if it had exceeded 50 cm in magnitude. This suggests that gradients in the total shear (S_T) as high as 0.09 probably do not extend more than 10 m or so beneath the surface (Figure 9), and the total shear below that depth must be more smoothly varying. This argument, however, only applies to the downdip extent of the slip variations seen at the surface. It does not preclude the existence of high slip gradients below 10 m depth, as long as they are not in-phase with the surficial slip gradients or with each other.

We now consider the possible depth extent of the kilometer-scale variations in slip. As an example, the slip gradient between the southern end of the central low-slip area (at 2.7 km) and the northern end of the southern high-slip area (at 3.5 km) is 0.002 (1.7 m change in slip over 800 m distance). Any local uplift or subsidence spread over this area could perhaps be as large as several meters or more without being easily visible. This suggests that kilometer-scale gradients in total shear (S_T) of the order of 0.002 may extend several kilometers beneath the surface (Figure 9).

6. Implications of Slip Variability in the Landers Earthquake for Estimates of Slip in Prehistoric Earthquakes on Other Faults

One purpose of this study was to document the degree of variability in slip along the main fault rupture for comparison with offset measurements along prehistoric ruptures. Determining the amount of slip in past earthquakes is important for characterizing the size and frequency of earthquakes along a fault. Offset geomorphic features are commonly used to estimate the amount of slip in prehistoric earthquakes [*Wallace*, 1968; *Clark*, 1970; *Sieh*, 1978; *Rockwell and Pinault*, 1986; *Zhang et al.*, 1987; *Lindvall et al*, 1989; *Zhang et al.*, 1990; *McGill and Sieh*, 1991; *Grant and Sieh*, 1993]. One source of error in using offset geomorphic features is the variability in slip that may occur in a single earthquake. A distribution of offsets along a prehistoric rupture can either be explained by a single slip event or by multiple slip events. *McGill and Sieh* [1991] used variability in slip along historical ruptures on strike-slip faults as a modern analog for prehistoric earthquake ruptures. However, the utility of this approach has been hampered by a lack of data on slip variability along historical earthquake ruptures. The closely spaced slip measurements presented here provide a more robust data set that documents slip variability within a single earthquake.

6.1. Potential Problems With Using Histograms to Determine the Number of Earthquakes Associated With Offset Geomorphic Features

One approach to estimating the number of slip events associated with offset features is to construct a histogram showing the number of features offset various amounts along a particular fault segment. *McGill and Sieh* [1991] used this method in a study of offset geomorphic features along the Garlock fault. They argued that if the offsets ranging between 2 and 6 m along the Garlock fault in Pilot Knob Valley had all formed in the most recent slip event, then one would expect the offsets to be distributed uniformly or unimodally within this range. The offsets ranging between 2 and 6 m in Pilot Knob Valley, however, are bimodally distributed (Figure 10a). For this reason, *McGill and Sieh* [1991] favored an interpretation in which features offset around 3 m were displaced in the most recent earthquake alone, whereas features offset 5-6 m were displaced in the past two slip events combined.

McGill and Sieh [1991] assumed that a histogram of offsets from a single earthquake would have a single peak, even though that peak might be very broad because of variability in the slip along the fault. Preliminary analysis of offsets that we measured along a 5.6-km length of the Emerson fault, however, indicates that offsets from a single earthquake can

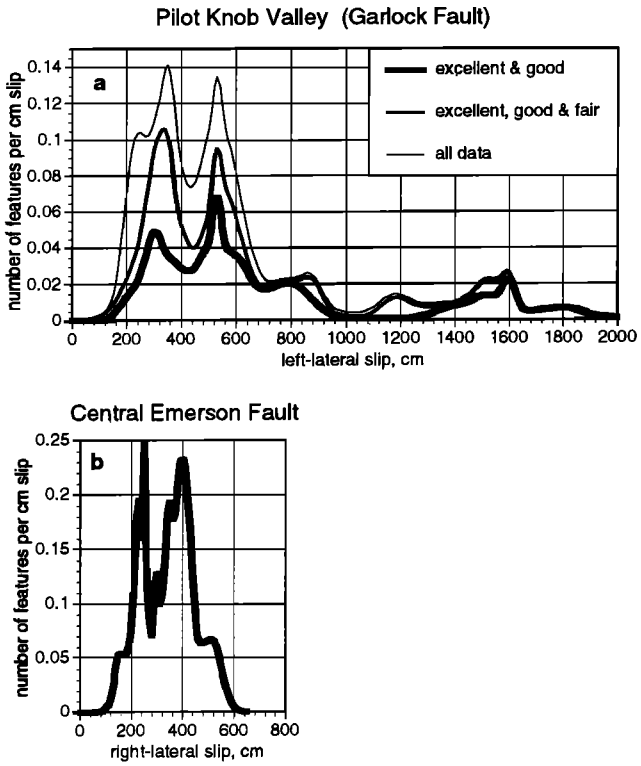

Figure 10. (a) Number of offset features per cm slip along the Garlock fault. (b) Number of offset features per centimeter slip along the portion of the Emerson fault that we mapped. To construct these plots, we treated each offset measurement as a Gaussian curve with a mean at the best estimate of the measurement and with a standard deviation equal to one-quarter the length of the error bar. The reported uncertainties are thus assumed to be $\pm 2\sigma$. The Gaussian curves for all the measurements were then summed to produce a figure similar to a histogram of offset measurements but including the information contained in the error bars of the measurements. The area beneath each peak represents the number of geomorphic or cultural features offset by the slip amounts spanned by the width of that peak. Along the Garlock fault the correlation of each offset feature across the fault was rated excellent, good, fair, or poor. Along the central Emerson fault we only measured offsets with good or excellent correlations.

produce a bimodal histogram, similar to the one for Pilot Knob Valley (Figure 10b).

In order to determine if offsets clustered in a bimodal distribution along other segments of the Landers rupture we used slip measurements in the SCEC database (see acknowledgments) to construct histograms for all of the faults that ruptured in the 1992 Landers earthquake. Most of the histograms for faults that ruptured in the Landers earthquake are multimodal (Figure 11). Many of the peaks are very narrow, however, and represent single measurements rather than clusters of measurements. These narrow peaks arise from sparse sampling of variable slip, and they emphasize the importance of closely spaced slip measurements along strike. The broader peaks (e.g., at 200 and 300 cm on the Homestead Valley fault), however, represent real clustering of the slip measurements, confirming that a multimodal histogram of offsets should not necessarily be interpreted as evidence for multiple earthquakes.

In some cases the different peaks in the histograms correspond to particular segments of the faults, suggesting that if a short enough fault segment is considered, a single rupture event may in fact produce a single-peaked histogram. The 5.6-km-long segment that produced the bimodal histogram shown in Figure 10b can be broken down into 1.5- to 2-km-long segments, some of which have histograms with one dominant peak, although they still have minor peaks at other offset values (Figure 12). Thus, at least for some parts of the rupture the multimodal nature of the histograms is produced by the kilometer-scale variations in slip. The fault lengths over which nearly unimodal histograms are observed are so short, however, as to be of little use in deciphering the number of prehistoric earthquakes associated with a set of offset geomorphic features.

6.2. Modification of the Histogram Approach: Subtracting a Running Average of Slip From Each Slip Measurement Before Constructing the Histogram

The long-wavelength variations in slip can be filtered out by subtracting a running average of the slip from each slip measurement. Thus peaks in the histogram that correspond to segments with uniform slip along strike will merge, even if the endpoints of the segments with uniform slip are not known. Furthermore, areas where slip is gradually increasing or decreasing, such as near the ends of a fault or between segments with uniform slip along strike, will also produce a unimodal histogram. The four main faults that ruptured in the Landers earthquake each produce a primarily unimodal histogram if a running average of the slip is subtracted from each slip measurement before constructing the histogram (Figure 13).

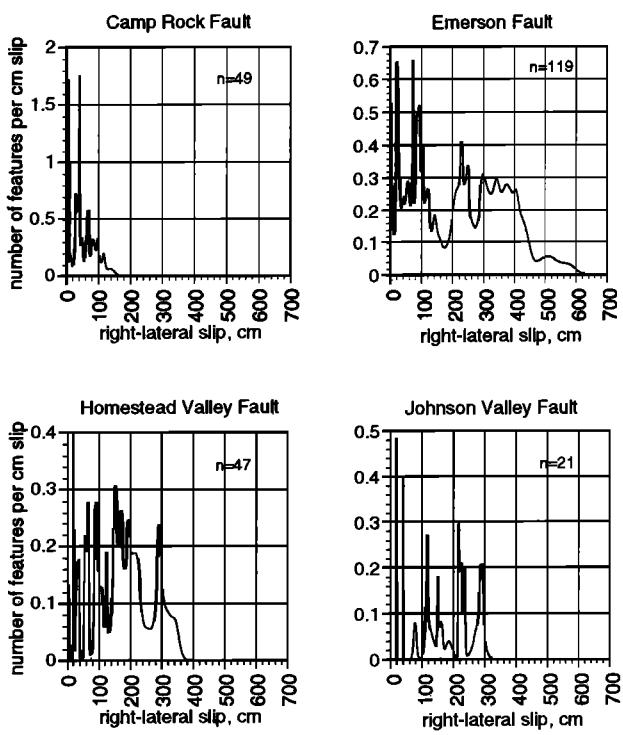

Figure 11. Number of offset features per centimeter of slip for each of the four major faults that ruptured in the Landers earthquake. See caption of Figure 10 for a discussion of how these plots were constructed. The number of measurements used in each plot is shown in the top right corner.

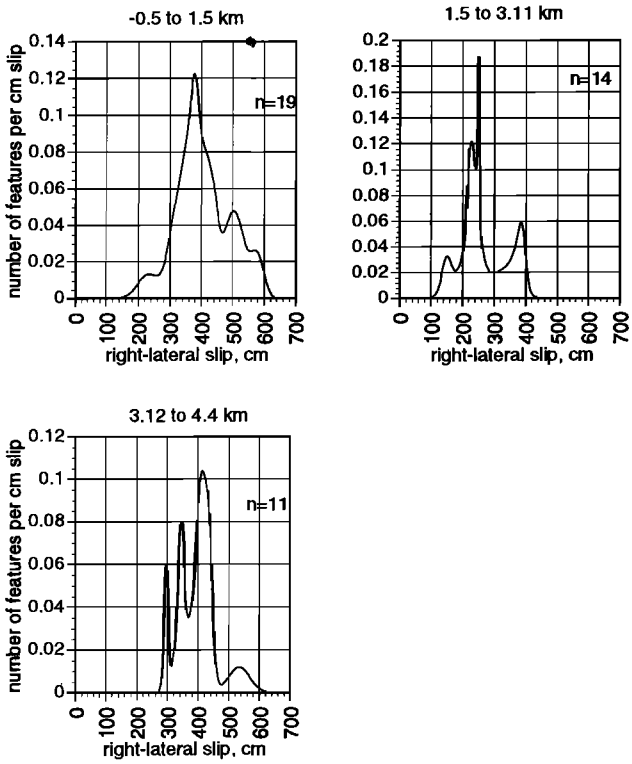

Figure 12. Number of offset features per centimeter of slip for short segments of the portion of the Emerson fault that we mapped. Distances shown at the top of each plot are measured southeastward from Galway Lake Road and indicate the portion of the fault included in each plot. Plots were constructed as described in the caption for Figure 10.

Although histograms of slip with a running average subtracted do produce a single peak when a single earthquake is considered, is this approach useful in determining the number of earthquakes represented in a set of slip measurements along a fault with prehistoric ruptures? To simulate a data set containing two earthquakes, we doubled the slip measurements from the Landers earthquake and from a hypothetical earthquake with a smoothly varying slip distribution. This is clearly an overly simplistic model for a two-event data set, but it is illustrative, nonetheless.

Figure 14 shows the histograms of slip with running average subtracted for several simulated two-event data sets. The histogram for the smoothly varying, hypothetical rupture (Figure 14b) is bimodal. Thus, for a rupture with smoothly varying slip, this approach is able to distinguish when two slip events are included in a set of slip measurements. For the Landers rupture, however, the fluctuation of slip about the running average is sufficiently large that this approach produces a roughly unimodal histogram (Figures 14d, 14f, and 14h), even though two events are included in these data sets. Therefore, if this approach is applied to slip measurements along prehistoric ruptures, a multimodal histogram probably indicates that more than one earthquake was involved, but a unimodal histogram does not necessarily mean that all the offsets were produced by a single earthquake.

As an example of the potential uses and limitations of this technique, we apply it to the geomorphic offsets along the Garlock fault in Pilot Knob Valley. We consider just those offsets that make up the two main peaks in Figure 10a (offsets < 7 m). If offsets of all qualities (excellent through poor) are included, the histogram with running average subtracted has one main peak with a split top, which could perhaps represent two different earthquakes (Figure 15a). If the offsets with poor correlations across the fault are excluded, however, the histogram with running average subtracted has a single main peak with minor side lobes (Figure 15b). Thus this approach is inconclusive when applied to the Pilot Knob Valley offsets. The split peak in Figure 15a is not convincing evidence for two events, and the single peak in Figure 15b does not necessarily mean that all offsets < 7 m were produced by a single earthquake, for the reasons discussed in the previous paragraph.

6.3. Potential Use of Slip Gradients to Determine the Number of Earthquakes Associated With Offset Geomorphic Features

Another method that *McGill and Sieh* [1991] used to distinguish features offset in a single event from those offset in multiple events was to compare the slip gradient required for a single event interpretation of a set of prehistoric offset features to the maximum slip gradients observed in historical ruptures. This approach assumes that if the slip gradient

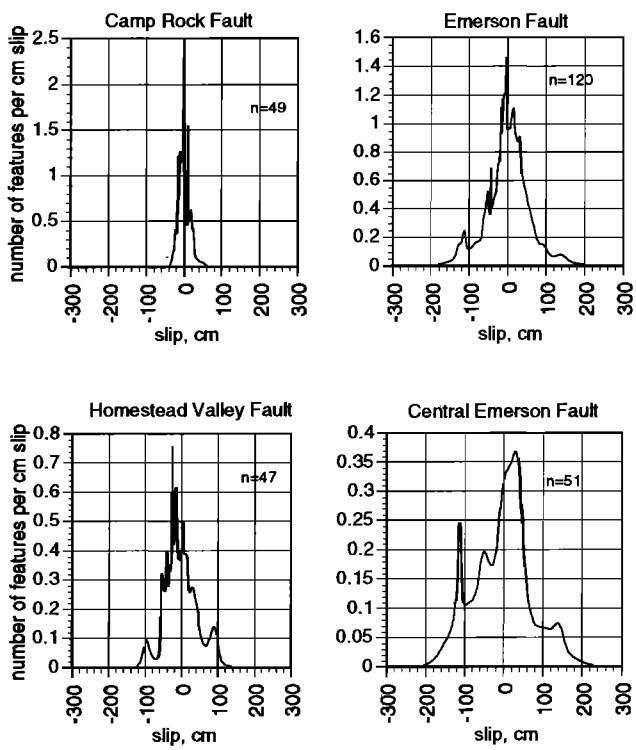

Figure 13. Number of offset features per centimeter of slip, with a running average of slip subtracted from each measurement. To construct these plots, a running average of the slip (including the two nearest points on each side of each measurement) was subtracted from each slip measurement, and then a histogram-like plot was made, as described in the caption to Figure 10. The plot labeled central Emerson fault includes only the measurements that we made on the 5.6-km length southeast of Galway Lake Road. The number of offset features included in each plot is shown in the top right corner. The plot for the Johnson Valley fault is not shown due to the sparsity of measurements available to us along that fault.

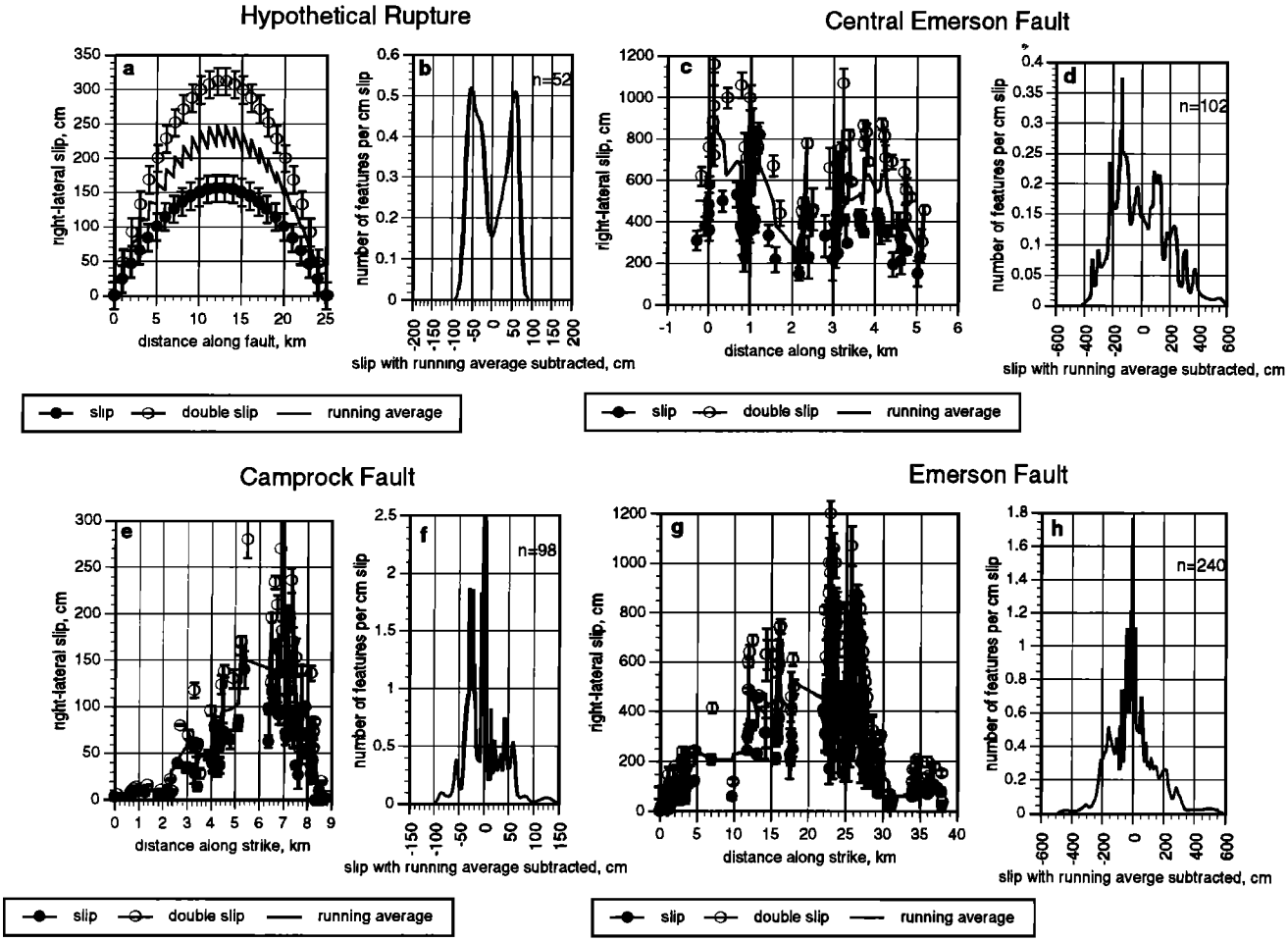

Figure 14. (a), (c), (e), and (g) Slip and doubled slip versus distance along strike and (b), (d), (f), and (h) plots showing number of offset features per centimeter slip, with running average of slip subtracted for a hypothetical rupture with smoothly varying slip (Figures 14a and 14b) and for portions of the Landers rupture (Figures 14c-14h). Figures 14b, 14d, 14f, and 14 h were constructed as described in the caption for Figure 13, but both the actual slip measurements and doubled slip measurements were used.

between any two slip measurements along a prehistoric rupture is larger than any slip gradient observed in historical earthquakes, then the larger of the two slip measurements along the prehistoric rupture probably represents more than one earthquake. *McGill and Sieh* [1991] used this approach

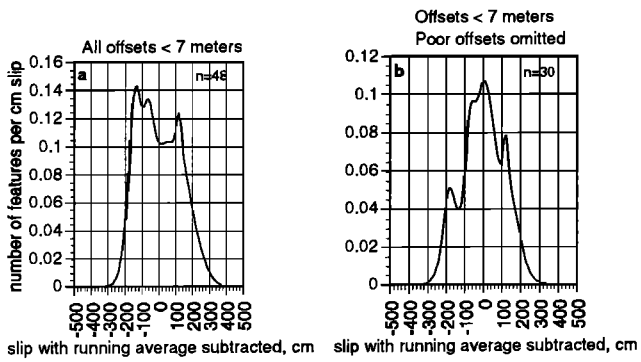

Figure 15. Number of offset features per centimeter slip, with a running average of slip subtracted, for the portion of the Garlock fault in Pilot Knob Valley. Plots were constructed as described in the caption for Figure 13. Only measurements ≤ 700 cm were included. (a) Including poor quality offsets and (b) omitting poor quality offsets.

to argue that geomorphic features offset around 3 m and a little over 5 m located within a few tens of meters from each other along the Garlock fault in eastern Pilot Knob Valley probably were not all offset in the most recent earthquake alone but that the 5-m offsets had required two earthquakes to form. At that time, however, most slip measurements reported from large, historical strike-slip earthquakes were spaced more than 100 m apart, so there were no observations available on how much single-earthquake slip could change over distances of a few tens of meters along strike. The 1992 Landers earthquake provides an opportunity to address this question.

Five pairs of offset features in Pilot Knob Valley have slip gradients that are larger than the largest slip gradients observed along the Landers earthquake rupture (Table 4). Three of these pairs involve offsets of around 2.5 and 8.5 m. The unprecedented slip gradients between these measurements suggest that offsets that form the third peak (at 8 to 8.5 m) in Figure 10a required more than one earthquake to form. The two remaining pairs involve offsets of around 3 m and 5-6 m. This indicates that even the Landers rupture does not provide a precedent for slip gradients as high as those required for a single-earthquake interpretation of the first two peaks in Figure 10a. Nonetheless, the slip gradients for the Emerson

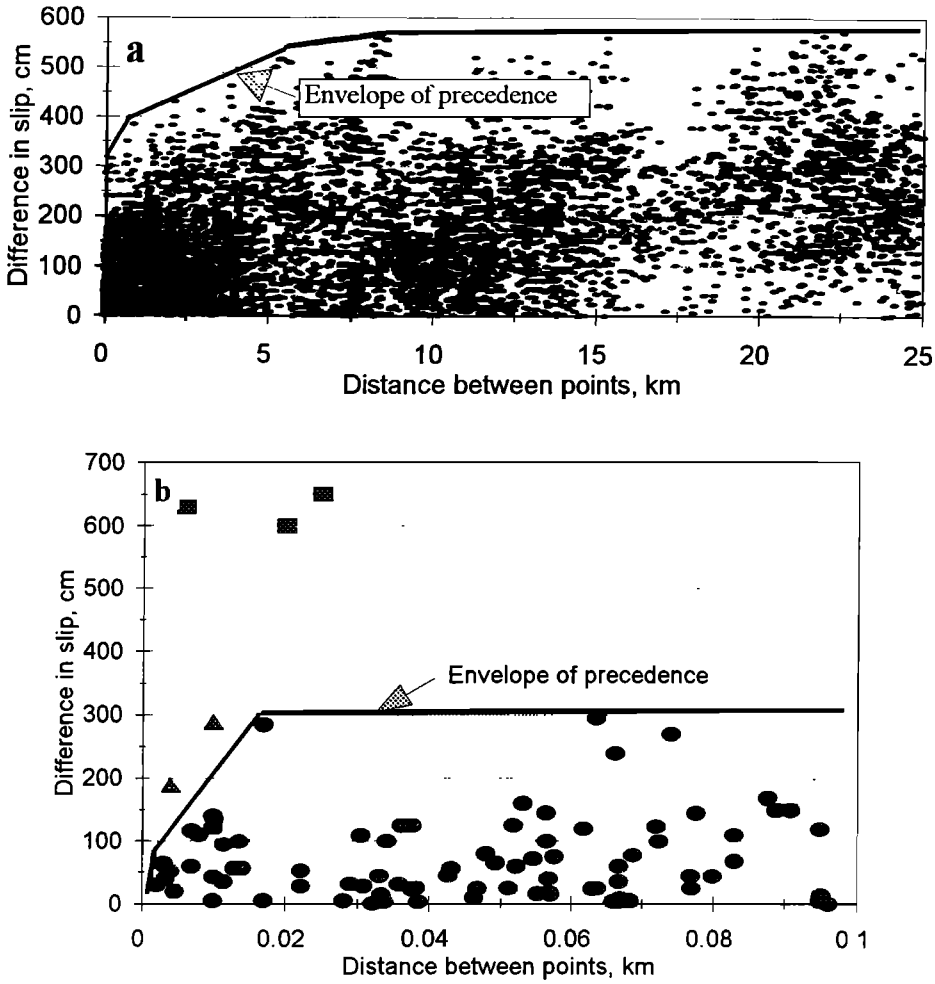

Figure 16. Difference in slip as a function of distance between offset measurements along the Emerson fault (a) for all measurements within 25 km of each other and (b) for all measurements within 100 m of each other. Each oval represents a pair of offset measurements. Note that all measurement pairs, not just adjacent pairs, have been included in these plots. The envelope of precedence indicates the most extreme change in slip that has been documented for any given distance between points. The slope of a diagonal line between any point on the plot and the origin represents the slip gradient between a pair of offset measurements. Triangles and squares in Figure 16b represent measurement pairs along the Garlock fault in Pilot Knob Valley that have slip gradients larger than the largest slip gradients along the 1992 Landers rupture. See text for further explanation.

fault reported in Table 4 are high enough to make it difficult to convincingly argue that the 5-6-m offsets along the Garlock fault required two earthquakes to form.

6.4. Change in Slip as a Function of Distance Between Points

The slip gradient measured between points a few tens or a few hundreds of meters apart clearly can not be extrapolated to points much farther apart. For example, the observed slip gradient of 0.09 between offsets that are 18 m apart (Table 4) can not be used as a precedent for a 9-m change in slip in a single earthquake over a 100-m distance along strike. Thus, rather than reporting the maximum slip gradient, it may be more useful to show the maximum observed change in slip as a function of distance between points (Figure 16). The three Garlock fault pairs involving 2.5- and 8.5-m offsets (squares in Figure 16b) clearly have no precedent along the Landers rupture, but perhaps they might if closely spaced measurements were made along a historical rupture with a maximum displacement of at least 8.5. Although the two pairs of Garlock fault offsets involving about 3 and 5-6 m (triangles in Figure 16b) are outside the envelope of precedence, they are close enough that it seems possible that they may have formed in a single earthquake.

6.5. Other Approaches

Clearly, neither the use of histograms nor the use of slip gradients will necessarily provide an unambiguous determination of the number of earthquakes associated with offset geomorphic features. Other approaches, such as the use of relative age indicators on offset geomorphic features, or stratigraphic investigations may be necessary in many cases. These approaches are both time consuming and expensive. One simple observation may help to guide the interpretation of some offset geomorphic features: in cases where there are multiple downstream channel or gully segments offset from a single source, the channel segments offset a larger amount must have been offset in more than one earthquake. Although

this configuration is somewhat rare, it has been found along several strike-slip faults [*Sieh*, 1978; *McGill and Sieh*, 1991]. For example, along the Garlock fault in eastern Pilot Knob Valley, a channel offset 2.5 m has an older downstream channel wall that is offset 8.8 m from the same source channel (features 2-63(2) and 2-63(3) of *McGill and Sieh*, [1991]). This unambiguously indicates that at least one of the features making up the third peak (at 8-8.5 m) in Figure 10a has been offset in more than one earthquake. This is not a trivial observation, since one could argue that the Garlock fault is long enough to produce an earthquake with 8.8 m of displacement [*Wells and Coppersmith*, 1994].

7. Conclusions

The 1992 Landers earthquake was associated with the longest surface rupture and the largest strike-slip displacement of any earthquake within the past several decades in North America. As such, it provided an excellent opportunity to study the nature of a fresh, strike-slip fault rupture. Slip was quite variable along the main trace of the rupture at distance scales ranging from a few kilometers to a few tens of meters. The slip variations over scales of a few tens of meters are probably the result of incomplete expression of the rupture in unconsolidated surficial materials. The kilometer-scale slip variations may be caused in part by such surficial effects, but the geometry of the fault may also play a role.

A significant amount of slip occurred on secondary fault strands up to 1.7 km away from the main trace. The orientation of the secondary fractures with different senses of slip fit a simple strain ellipse defined by right lateral shear along a north-northwest striking shear zone. Although up to 110 cm of right-lateral slip occurred on secondary fractures in some areas, the slip on secondary fractures did not compensate for the variations in slip along the main rupture zone.

The presence of uplifted, older alluvial fan surfaces and Plio-Pleistocene sediments attests to previous Late Quaternary activity on the central Emerson fault. Crude age constraints on these surfaces and deposits suggest recurrence intervals that are consistent with the 9-kyr interval documented in a paleoseismic trench [*Rubin and Sieh*, 1997]. The sense of vertical slip in the 1992 earthquake varied along strike, but it was consistent with the sense of vertical slip in prehistoric earthquakes, as inferred from the locations of areas of uplifted, older alluvium.

The variability of slip along the ruptures associated with the Landers earthquake calls for caution in interpreting geomorphic offsets along prehistoric fault ruptures. *McGill and Sieh's* [1991] method of using histograms to distinguish the number of earthquakes associated with particular offset features is not always valid but may be useful in some cases if a running average is subtracted from the offset measurements before the histogram is constructed. The slip gradients between offset measurements along the Landers rupture were large enough that it will be difficult to use slip gradients to demonstrate that offset features along a prehistoric rupture formed in different numbers of events. Therefore other methods must be developed to distinguish the number of earthquakes associated with offset geomorphic features along prehistoric fault ruptures.

The slip variability documented along the Landers earthquake weakens the arguments that *McGill and Sieh* [1991] made for interpreting the 5-6-m offsets along the Garlock fault as representing the amount of slip in two earthquakes. Whether these offsets represent the slip in one or two earthquakes remains ambiguous.

Acknowledgments. We thank Kenneth Hudnut, Scott Lindvall, Kerry Sieh and his 1992 field mapping class, James Spotila, Joann Stock, Brian Wernicke, Doug Yule, and Judith Zachariasen for making available their measurements along other portions of the Landers rupture. We thank Anne Lilje for compiling the measurements of these other scientists into the SCEC database and for helping us to access that database. Dawn Grant, Mike Slates, Joseph Stroud, Sarah Tegt, and Amanda Wilcox assisted with surveying and with some of the offset measurements. Malcolm Clark (U.S. Geological Survey) provided the 1:6000 scale aerial photographs on which we mapped. We thank Tom Heaton and Harold Magistrale for helpful reviews of this manuscript. Discussions with John McGill and Kerry Sieh were also very helpful. This research was supported by the Southern California Earthquake Center. SCEC is funded by NSF Cooperative Agreement EAR-8920136 and USGS Cooperative Agreements 14-08-0001-A0899 and 1434-HQ-97-AG01718. SCEC contribution 277.

References

Ambraseys, N. N., and J. S. Tchalenko, The Dasht-e Bayaz (Iran) earthquake of August 31, 1968: A field report, *Bull. Seismol. Soc. Am., 59*, 1751-1792, 1969.

Ambraseys, N. N., and A. Zatopek, The Mudurnu Valley, West Anatolia, Turkey, earthquake of 22 July 1967, *Bull. Seismol. Soc. Am., 59*, 521-589, 1969.

Arrowsmith, R., and D. D. Rhodes, Original forms and initial modifications of the Galway Lake Road scarp formed along the Emerson fault during the 28 June 1992 Landers, California, earthquake, *Bull. Seismol. Soc. Am., 84*, 511-527, 1994.

Aydin, A., and Y. Du, Surface rupture at a fault bend: The 28 June 1992 Landers, California, earthquake, *Bull. Seismol. Soc. Am., 85*, 111-128, 1995.

Aydin, A., M. Antonellini, R. Arrowsmith, P. Christiansen, M. Cooke, K. Cruikshank, Y. Du, D. Pollard, H. Wu, and A. Sarna-Wojcicki, Surface rupture associated with the June 28 1992 Landers, California, earthquake, along the north-central Emerson fault and its neotectonic significance, *Eos Trans. AGU, 73*(43), Fall Meet. Suppl., 381, 1992.

Bonilla, M. G., and J. J. Lienkaemper, Visibility of fault strands in exploratory trenches and timing of rupture events, *Geology, 18*, 153-156, 1990.

Bucknam, R. C., G. Plafker, and R. V. Sharp, Fault movement (afterslip) following the Guatemala earthquake of February 4, 1976, *Geology, 6*, 170-173, 1978.

Bull, W. B., Global climate change and active tectonics: Effective tools for teaching and research, *Geomorphology, 16*, 217-232, 1996.

Clark, M. M., Some characteristics of the most recently active traces of the Garlock fault, *Geol. Soc. Am. Abstr. Programs, 2*, 82, 1970.

Clark, M. M., Surface rupture along the Coyote Creek fault, *U.S. Geol. Surv. Prof. Pap., 787*, 55-86, 1972.

Cohee, B. P., and G. C. Beroza, Slip distribution of the 1992 Landers earthquake and its implications for earthquake source mechanics, *Bull. Seismol. Soc. Am., 84*, 692-712, 1994.

Das, S., and K. Aki, Fault plane with barriers: A versatile earthquake model, *J. Geophys. Res., 82*, 5658-5670, 1977.

Deng Q., Chen S., Song F. Zhu S. Wang Y., Zhang W., Jiao D., B. C. Burchfiel, P. Molnar, L. Royden, and Zhang P., Variations in the geometry and amount of slip on the Haiyuan (Nanxihauchan) fault zone, China and the surface rupture of the 1920 Haiyuan earthquake, in *Earthquake Source Mechanics, Geophys. Monogr. Ser.*, vol. 37, edited by S. Das, J. Boatwright, and C. H. Scholz, pp. 169-182, AGU, Washington, D. C., 1986.

Dibblee, T. W., Jr., Geological map of the Rodman Mountains Quadrangle, San Bernardino County, California, *U.S. Geol. Surv. Misc. Geol. Invest. Map, I-430*, 1964.

Grant, L. B., and K. Sieh, Stratigraphic evidence for seven meters of dextral slip on the San Andreas fault during the 1857 earth-

quake in the Carrizo Plain, *Bull. Seismol. Soc. Am., 83*, 619-635, 1993.

Hart, E. W., W. A. Bryant, and J. A. Treiman, Surface faulting associated with the June 1992 Landers earthquake, California, *Calif. Geol., 46*(1), 10-16, 1993.

Heaton, T., Evidence for and implications of self-healing pulses of slip in earthquake rupture, *Phys. Earth Planet. Inter., 64,* 1-20, 1990.

Irvine, P. J., and R. L. Hill, Surface rupture along a portion of the Emerson fault, *Calif. Geol., 46*(1), 23-26, 1993.

Johnson, A. M., R. W. Fleming, and K. M. Cruikshank, Shear zone formed along long, straight traces of fault zones during the 28 June 1992 Landers, California, earthquake, *Bull. Seismol. Soc. Am., 84,* 499-510, 1994.

Lazarte, C. A., J. D. Bray, A. M. Johnson, and R. E. Lemmer, Surface breakage of the 1992 Landers earthquake and its effects on structures, *Bull. Seismol. Soc. Am., 84,* 547-561, 1994.

Lees, J. M., and C. Nicholson, Three-dimensional tomography of the 1992 southern California earthquake sequence: Constraints on dynamics of earthquake rupture?, *Geology, 21*, 387-390, 1993.

Lindvall, S. C., T. K. Rockwell, and K. W. Hudnut, Evidence for prehistoric earthquakes on the Superstition Hills fault from offset geomorphic features, *Bull. Seismol. Soc. Am., 79,*342-361, 1989.

McGill, S. F., and K. E. Sieh, Surficial offsets on the central and eastern Garlock fault associated with prehistoric earthquakes, *J. Geophys. Res., 96,* 21,597-21,621, 1991.

Michael, A. J., and D. Eberhart-Phillips, Relations among fault behavior, subsurface geology, and three-dimensional velocity, *Science, 253*, 651-654, 1991.

Nowroozi, A. A., and A. Mohajer-Ashjai, Faulting of Kurizan and Koli (Iran) earthquakes of November 1979: A field report, *Bull. Bur. Rech. Geol. Min., Sect. 4, 2*, 91-99, 1981.

Revenaugh, J., Relation of the 1992 Landers, California, earthquake sequence to seismic scattering, *Science, 270*, 1344-1347, 1995.

Rockwell, T. K., and C. T. Pinault, Holocene slip events of the southern Elsinore fault, Coyote Mountains, Southern California, in *Neotectonics and Faulting in Southern California: Guidebook for the Cordilleran Section Meeting in Los Angeles*, pp. 193-196, Cordilleran Sect., Geol. Soc. of Am., Fresno, Calif., 1986.

Rubin, C. M., and K. Sieh, Long dormancy, low slip rate and similar slip per event for the Emerson fault, Eastern California Shear Zone, *J. Geophys. Res., 102*, 15319-15333, 1997.

Sharp, R. V., Comparison of 1979 surface faulting with earlier displacements in the Imperial Valley, in *The Imperial Valley, California, Earthquake of October 15, 1979, U.S. Geol. Surv. Prof. Pap., 1254,* 213-221, 1982.

Sharp, R. V., et al., Surface faulting in the central Imperial Valley, in *The Imperial Valley, California, Earthquake of October 15, 1979, U.S. Geol. Surv. Prof. Pap., 1254,* 119-143, 1982.

Sibson, R. H., Rupture interaction with fault jogs, in *Earthquake Source Mechanics, Geophys. Monogr. Ser.*, vol. 37, edited by S. Das, J. Boatwright, and C. H. Scholz, pp. 157-168, AGU, Washington, D. C., 1986.

Sieh, K. E., Slip along the San Andreas fault associated with the great 1857 earthquake, *Bull. Seismol. Soc. Am., 68*, 1421-1448, 1978.

Sieh, K., et al., Near-field investigations of the Landers earthquake sequence, April to July 1992, *Science, 260,* 171-176, 1993.

Tchalenko, J. S., and M. Berberian, Dasht-e Bayaz fault, Iran: Earthquake and earlier related structures in bed rock, *Geol. Soc. Am. Bull., 86*, 703-709, 1975.

Thatcher, W., and M. Lisowski, Long-term seismic potential of the San Andreas fault southeast of San Francisco, California, *J. Geophys. Res., 92,* 4771-4784, 1987.

Toksoz, M. N., E. Arpat, and F. Saroglu, East Anatolian earthquake of 24 November 1976, *Nature, 270,* 423-425, 1977.

Wald, D. J., and T. H. Heaton, Spatial and temporal distribution of slip for the 1992 Landers, California, Earthquake, *Bull. Seismol. Soc. Am., 84,* 668-691, 1994.

Wallace, R. E., Notes on stream channels offset by the San Andreas fault, southern Coast Ranges, California, in *Proceedings of Conference on Geological Problems of the San Andreas Fault System,* edited by W. R. Dickenson and A. Grantz, *Stanford Univ. Publ. Geol., 11,* 6-21, 1968.

Wells, D. L., and K. J. Coppersmith, New empirical relationships among magnitude, rupture length, rupture width, rupture area and surface displacement, *Bull. Seismol. Soc. Am., 84,* 974-1002, 1994.

Williams, P. W., and H. W. Magistrale, Slip along the Superstition Hills fault associated with the 24 November 1987 Superstition Hills, California, earthquake, *Bull. Seismol. Soc. Am., 79,* 390-410, 1989.

Yeats, R., K. Sieh, and C. R. Allen, *The Geology of Earthquakes*, Oxford Univ. Press, New York, 1997.

Zachariasen, J., and K. Sieh, The transfer of slip between two en echelon strike-slip faults: A case study from the 1992 Landers earthquake, southern California, *J. Geophys. Res., 100,* 15,281-15,301, 1995.

Zhang, P., M. Ellis, D. B. Slemmons, and F. Mao, Right-lateral displacement and the Holocene slip rate associated with prehistoric earthquakes along the southern Panamint Valley fault zone: Implications for southern basin and range tectonics, *J. Geophys. Res., 95*, 4857-4872, 1990.

Zhang, W., D. Jiao, P. Zhang, P. Molnar, B. C. Burchfiel, Q. Deng, and Y. Wang, Displacement along the Haiyuan fault associated with the great 1920 Haiyuan, China, earthquake, *Bull. Seismol. Soc. Am., 77,* 117-131, 1987.

S. F. McGill, Department of Geological Sciences, California State University, San Bernardino, 5500 University Parkway, San Bernardino, CA 92407. (e-mail: smcgill@csusb.edu)

C. M. Rubin, Department of Geology, Central Washington University, Ellensburg, WA 98926. (e-mail: charlier@geology.cwu.edu)

(Received July 29, 1997; revised April 14, 1998;
accepted May 4, 1998.)